Gravitational Lensing

Mai Samir Adly Rizk

University of Cape Town

Supervised by:
Doctor Alvaro de la Cruz-Dombriz
Department of Mathematics and Applied Mathematics

February 2023

A dissertation submitted in full fulfilment of the requirements for the degree of Master of Science by Research in the Department of Mathematics and Applied Mathematics

Abstract

Gravitational lensing derives its simplicity from some basic assumptions that are satisfied by most physical situations.The thin lens approximation and weak field approximations were used to build the whole theory and explain the phenomenology up to today. We review the gravitational lensing formalism in weak and strong limits. We discuss the main results of massive dark objects at galactic center as Schwarzschild black hole lenses. We also demonstrate the gravitational lensing analysis in $f(R)$ gravity theories. We compare our results with GR. We find some interesting results for $f(R) = R^{1+\delta}$ in weak limit.

Declaration

I, the undersigned, hereby declare that the work contained in this research project is my original work and that any work done by others or by myself previously has been acknowledged and referenced accordingly.

Signed by candidate

Mai Samir Adly Rizk, February 2023

Contents

1. Introduction

The study of the deflection of light has its origin in ancient times. It dates back to the eighteenth century when the nature of light was the center of attention(Meneghetti, 2021). Sir Issac Newton described the light as particles that move along a linear paths in space after being emitted from luminous bodies. According to the classical laws of mechanics these light particles would be affected by gravity and would experience attraction forces from other massive particles. Scholars at this time started being more interested in studying how the trajectories of light particles would change under the effect of the gravitational attraction of massive bodies. They performed calculations, using classical mechanics laws, on the trajectories of light that passes at distance r near a mass M to find that they experience a deflection angle equal to

$$\hat{\alpha}(r) = \frac{2GM}{rc^2}, \tag{1.0.1}$$

Where G is the universal gravitational constant and c is the speed of light.

In the early twentieth century, Einstein developed his General Theory of Relativity which predicted the deflection angle of light. He evaluated the deflection angle once again using his theory and found out that its value is twice the Newtonian deflection angle

$$\hat{\alpha}(r) = \frac{4GM}{rc^2}. \tag{1.0.2}$$

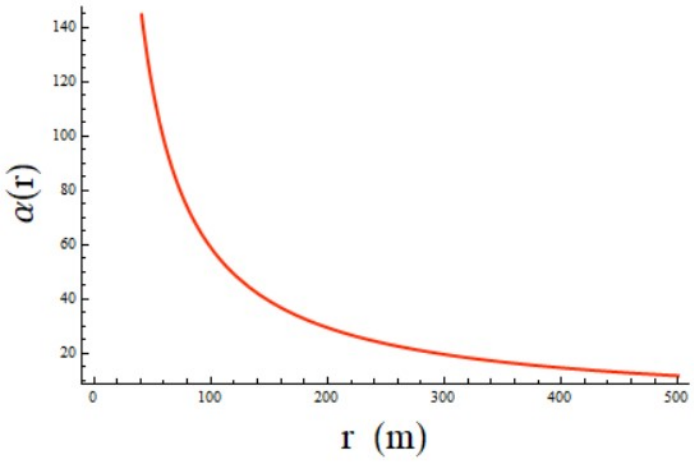

Figure 1.1: Deflection angle $\alpha(r)$ (1.0.2) in radians against the distance d where $r = d$ from the sun $M_\odot$

We can see in Fig. 1.1 that the deflection angle depends on the distance d. The larger the distance is from the Sun the smaller the deflection angle. Einstein's general theory of relativity prediction of deflection angle was confirmed after several attempts to measure it during a solar ellipse. In 1919, it was confirmed by two expeditions that the Royal Astronomical Society organized. They took photographs of the stars around the Sun during the solar eclipse and compared them with other photographs of the same region of the sky when the Sun was not in this region anymore. The deflection angle was measured and it was confirmed that the light can be deflected by gravity. The results were matching

with the theory of general relativity and not with Newtonian physics. Astronomers were able to improve the accuracy of these measurements over the next half century as eclipse measurements were repeated over and over again. It was possible to observe how some masses act as gravitational lenses by studying the deflection of light by massive bodies. This term "lens" was first used by O.J. Lodge, who mentioned that we should not consider the solar gravitational field as a lens since it has no focal length Lodge (1919). In contrast to an optical lens, light traveling near the center of a point-like gravitational lens is deflected most, while light traveling farther from it is deflected the least. Gravitational lenses, therefore, do not have a single focal point, but rather a focal line. The case where the source of light, the massive gravitational lens, and the observer are in perfect alignment was studied and the source would appear as a ring around the massive gravitational lens but a misalignment will result in the observer seeing an arc segment. The ring is referred to as *"Einstein's ring"*. This phenomenon happens because the light can travel in various trajectories before reaching the observer.

Different various types of gravitational lenses have been studied over the years. Fritz Zwicky was the first to speculate that the newly discovered galaxies (which at the time were called 'nebulae') might act as both sources and lenses, which would be much more likely to be observed due to their large masses and sizes Zwicky (1937). Among Zwicky's key contributions to gravitational lensing (GL)theory is the possibility of understanding how matter is distributed in the lenses by using this phenomenon. Moreover, Zwicky realized in during the years, galaxies move in clusters at incredible speeds that are not explained by the existence of observable matter only. It was necessary to postulate that the galaxy cluster held a significant amount of invisible mass that is able to produce a much stronger gravitational attraction force than that caused by just visible matter. he named it *"missing mass"*, which we call it nowadays *"dark matter"*. He had the impression that this massive invisible mass would have caused GL phenomena. As astronomy advances, gravitational lens masses have become a standard tool to determine the masses of cosmic objects, as well as the structure and size scale of the universe. We will review the GL analysis in both weak and strong limits in the second chapter. We will go through the formalism in detail. We will derive the lens equation in both weak and strong fields. Furthermore, we will explore the different gravitational lensing parameters such as the image positions and magnifications in both fields.

The recent observational data interpretation within the framework of General Relativity (GR) requires us to introduce unknown dark matter and dark energy in order to assist in understanding the self-gravitating astrophysical structures and the problem of cosmic acceleration. It has, however, been the price of preserving the simplicity of Hilbert-Einstein's Lagrangian that some odd-behaving physical entities have been introduced which have been, until now, unexplored by experimental means at fundamental scales. In light of this, several alternative gravity theories have been developed in order either to recover the validity of GR at any scale or to generalize Einstein's theory in a suitable manner. Moreover, an unparalleled window into gravitational lensing in the strong gravity regime has begun as a result of the recent Event Horizon Telescope photos of black holes and their shadows. For the first time, measurements from the Event Horizon Telescope allowed for the visualization of light emission and deflection by the surrounding accretion desk of a black hole. In the near future, we will be able to test any deviations from classical General Relativity BH solutions Guo et al. (2022).

Extended Theories of Gravity (ETGs) are important due to their basic assumptions being similar to GR with some corrections. The scalar-tensor theories are one of the most important ETGs, in which the gravitational action contains not only the metric but also a scalar field that contributes to the gravitational field. Because the scalar field is not coupled to the metric, we can still refer to it as a metric theory. The scalar field is only a component of the gravitational field's generation, and matter only responds to the metric, so free particles follow geodesics. Another intriguing class of ETGs considers the

modification of gravitational action to be dependent on curvature invariants. The so-called $f(R)$ theories Sotiriou (2006) are one example of taking the Lagrangian as a general function of scalar curvature. We are interested in $f(R)$ theories, and we shall go over the field equations in detail in the third chapter. However, the analysis of GL in those gravity theories is our primary focus. Thus, in the first chapter, we will go over the GL in GR in both the weak and strong limits for the massive dark object (MDO) at the center of the galaxy as a Schwarzschild black hole lens in detail. In the following chapter, we investigate the GL in $f(R)$ and compare it to our GR results. We demonstrate the formalism for $f(R) = R^n$ in detail and compare our results with GR.

2. Gravitational lensing in General Relativity

Gravity affects light, accordingly to the theory of General Relativity. Gravitational lensing refers to the phenomenon of light being deflected by a gravitational field. The objects that deflects the light are called gravitational lenses. Gravitational lenses are distributions of matter (such as galaxies or cluster of galaxies) between distant light sources and observers that bend light from the source as it travels toward them. By creating a gravitational field, it distorts and magnifies light from distant galaxies behind it that are in the same line of sight as it. It is as if you are looking through a giant magnifying glass. It provides researchers with the ability to observe details of early galaxies that are too far away to be seen with current technology. The GL theory was developed over the years and GR phenomenology of GL in weak limit has passed experimental tests. However, the scientific community, over last years, have been more interested in studying the deflection of light in strong fields. The potential to test the full GR in a regime where the differences with non-standard theories would be obvious, aiding in the differentiation between the various theories of gravitation, emphasizes the significance of GL in strong fields Esposito-Farèse (2004). The lensing characteristics close to the photon sphere, or the strong field limit, have drawn interest from the scientific community for this reason. Moreover, it may be possible to study the areas immediately outside of the event horizon thanks to the characteristics of the relativistic images. Relativistic images of black holes may be detectable by VLBI Doeleman et al. (2009), and information about strong fields contained within these new observables may be retrieved. We are going to study a point source GL due to light deflections in both weak and strong gravitational fields, using the Virbhadra & Ellis Virbhadra and Ellis (2000) lens equation and how they modeled the massive dark object (MDO) at the center of the galaxy as a Schwarzschild black hole lens. We will review in the next few sections the formulation of GL by the galactic MDO in weak limit and strong limit. The MDO has the mass $M = 3.61 \times 10^6 M_\odot$ and its distance away from us is $D_d = 7.62kpc$ Eisenhauer et al. (2005). Thus, we have $M/D_d \approx 2.26 \times 10^{-11}$ since we take natural units for which the gravitational constant $G = 1$ and the speed of light $c = 1$ so that $M \equiv MG/c^2$.

2.1 Weak limit

From the GR field equations, light deflection can be calculated by examining geodesic curves. It turns out that, just like in geometrical optics, Fermat's principle can be used to describe light deflection. We make an effort to approach the deflection of light as a refraction issue within the context of GR Meneghetti (2021). Fermat's principle of least action states that light travels in the path of the shortest time. As in geometrical optics, we require a refractive index n.

$$t_{travel} = \int \frac{n}{c} \mathrm{d}l, \tag{2.1.1}$$

where the shortest path between starting point A and ending point B is

$$\delta \int_A^B n(x(\vec{l}))\mathrm{d}l = 0 \tag{2.1.2}$$

We start now to find the equation of motion of the system by using Euler-Lagrange equation. In this case we choose the arbitrary curve parameter λ

$$\mathrm{d}l = \left|\frac{\mathrm{d}\vec{x}}{\mathrm{d}\lambda}\right| \mathrm{d}\lambda. \tag{2.1.3}$$

Assuming that λ is time we have

$$\delta \int_{\lambda_A}^{\lambda^B} n[\vec{x}(\lambda)] \left| \frac{\mathrm{d}\vec{x}}{\lambda} \right| \mathrm{d}\lambda = 0, \tag{2.1.4}$$

where

$$\dot{\vec{x}} = \left| \frac{\mathrm{d}\vec{x}}{\lambda} \right|.$$

We find our Euler equation as follows

$$\frac{\partial L}{\partial \vec{x}} - \frac{\mathrm{d}}{\mathrm{d}\lambda} \frac{\partial L}{\partial \dot{\vec{x}}} = 0 \tag{2.1.5}$$

where

$$L(\dot{\vec{x}}, \vec{x}, \lambda) = n[\vec{x}(\lambda)] \left| \frac{d\vec{x}}{\lambda} \right|. \tag{2.1.6}$$

Now, we find

$$\begin{aligned} \frac{\partial L}{\partial \vec{x}} &= |\dot{\vec{x}}| \frac{\partial n}{\partial \vec{x}} = (\vec{\nabla} n) |\dot{\vec{x}}| \\ \frac{\partial L}{\partial \dot{\vec{x}}} &= n \frac{\dot{\vec{x}}}{|\dot{\vec{x}}|}. \end{aligned} \tag{2.1.7}$$

We can see that $|\dot{\vec{x}}|$ is a tangent vector to the light path so we can normalize it and assume that $|\dot{\vec{x}}| = 1$. The unit tangent vector of the path can be written as $\vec{a} \equiv \dot{\vec{x}}$. Thus we have

$$\frac{\mathrm{d}}{\mathrm{d}\lambda}(n\vec{a}) - \vec{\nabla} n = 0, \tag{2.1.8}$$

or

$$n\dot{\vec{a}} = \vec{\nabla} n - \vec{a}(\vec{\nabla} n.\vec{a}), \tag{2.1.9}$$

where the right hand side in Eq. (2.1.9) can be written as the gradient of n perpendicular to the light path $\vec{\nabla}_\perp n$. Thus,

$$\dot{\vec{a}} = \frac{1}{n} \vec{\nabla}_\perp n = \vec{\nabla}_\perp \ln n. \tag{2.1.10}$$

We will make the following assumptions in order to find the refractive index. We will assume that we have a weak lens whose gravitational potential Φ is smaller than c^2, $\Phi/c^2 \ll 1$. We also assume that the light deflection takes place in a location that is small enough for us to ignore the expansion of the universe. We will choose a local flat inertial frame which is Minkowski's space-time. The line element is

$$\mathrm{d}s^2 = \eta_{\mu\nu} \mathrm{d}x^\mu \mathrm{d}x^\nu = c^2 \mathrm{d}t^2 - (\mathrm{d}\vec{x})^2, \tag{2.1.11}$$

where the metric is

$$\eta_{\mu\nu} = \begin{pmatrix} 1 & 0 & 0 & 0 \\ 0 & -1 & 0 & 0 \\ 0 & 0 & -1 & 0 \\ 0 & 0 & 0 & -1 \end{pmatrix} \tag{2.1.12}$$

By perturbing this metric with a weak lens, we have

$$\eta_{\mu\nu} \to g_{\mu\nu} = \begin{pmatrix} \left(1 + \frac{2\Phi}{c^2}\right) & 0 & 0 & 0 \\ 0 & -\left(1 - \frac{2\Phi}{c^2}\right) & 0 & 0 \\ 0 & 0 & -\left(1 - \frac{2\Phi}{c}\right) & 0 \\ 0 & 0 & 0 & -\left(1 - \frac{2\Phi}{c}\right) \end{pmatrix} \tag{2.1.13}$$

By finding a spherically symmetrical and static solution for Einstein's field equations, we find *Schwarzschild* metric

$$\mathrm{d}s^2 = \left(1 + \frac{2GM}{Rc^2}\right) c^2 \mathrm{d}t^2 - \left(1 - \frac{2GM}{Rc^2}\right)^{-1} \mathrm{d}R^2 - R^2(sin^2\theta \mathrm{d}\phi^2 + \mathrm{d}\theta^2) \tag{2.1.14}$$

We can then define a radial coordinate as follows

$$R = r\left(1 + \frac{GM}{2rc^2}\right)^2 \tag{2.1.15}$$

Thus our metric in Cartesian coordinates will be

$$\mathrm{d}s^2 = \left(\frac{1 - GM/2rc^2}{1 + GM/2rc^2}\right)^2 c^2 \mathrm{d}t^2 - \left(1 + \frac{GM}{2rc^2}\right)^4 (\mathrm{d}x^2 + \mathrm{d}y^2 + \mathrm{d}z^2) \tag{2.1.16}$$

We can see that in weak limit, $\Phi/c^2 = -GM/rc^2 \ll 1$,

$$\left(\frac{1 - GM/2rc^2}{1 + GM/2rc^2}\right)^2 \approx \left(1 - \frac{2GM}{rc^2}\right) = \left(1 + \frac{2\Phi}{c^2}\right)$$

and

$$\left(1 + \frac{GM}{2rc^2}\right)^4 \approx \left(1 + \frac{2GM}{rc^2}\right) = \left(1 - \frac{2\Phi}{c^2}\right)$$

Light travel along a null geodesics so we have $\mathrm{d}s = 0$ from which we obtain

$$\left(1 + \frac{2\Phi}{c^2}\right) c^2 \mathrm{d}t^2 = \left(1 - \frac{2\Phi}{c^2}\right) (\mathrm{d}\vec{x})^2 \tag{2.1.17}$$

Thus, we can find that the speed of light in gravitational field $c^{'}$ and the refractive index equals to

$$c' = \frac{|\mathrm{d}\vec{x}|}{\mathrm{d}t} = c\sqrt{\frac{1 + \frac{2\Phi}{c^2}}{1 - \frac{2\Phi}{c^2}}} \approx c\left(1 + \frac{2\Phi}{c^2}\right), \tag{2.1.18}$$

$$n = \frac{c}{c'} = \frac{1}{1 + \frac{2\Phi}{c^2}}, \tag{2.1.19}$$

where we can see that when $\Phi \leq 0$ then $n \geq 1$, and that the speed of light $c^{'}$ is smaller than it would be in the absence of the gravitational potential.

Now, we can see that eq.(2.1.10) can be written as

$$\dot{\vec{a}} \approx -\frac{2}{c^2}\vec{\nabla}_{\perp}\Phi \tag{2.1.20}$$

where $n = 1 - 2\Phi/c^2$ and $\Phi/c^2 \ll 1$ so $\ln n \approx -2\Phi/c^2$.

Finally, we can define our deflection angle as the integral over $-\dot{\vec{a}}$ along the light path,

$$\hat{\vec{\alpha}} = \vec{a}_{in} - \vec{a}_{out} = \frac{2}{c^2}\int_{\lambda_A}^{\lambda_B} \vec{\nabla}_{\perp}\Phi \mathrm{d}\lambda, \tag{2.1.21}$$

where $\vec{\nabla\Phi}$ points away from the lens center, so $\hat{\vec{\alpha}}$ points in the same direction.

The equation for $\hat{\vec{\alpha}}$ is not helpful as written because we would need to integrate over the actual light path. However, given that $\Phi/c^2 < 1$ we have a small deflection angle. Thus, the Born approximation can then be used to approximate the gravitational potential along the deflected trajectory by the potential along the un-deflected trajectory. We can integrate the gradient over the un-deflected light path, or along the z direction, using this approximation. The deflection angle is then given by

$$\hat{\vec{\alpha}}(J) = \frac{2}{c^2}\int_{-\infty}^{+\infty} \vec{\nabla}_\perp \phi(\theta, Z)\mathrm{d}Z. \tag{2.1.22}$$

where, for a point mass,$\Phi = -GM\sqrt{J^2+z^2}$, this means that our deflection angle will take this well known form

$$\hat{\vec{\alpha}}(J) = \frac{4GM}{c^2 J}\vec{a}_J = \frac{4GM}{c^2 J^2}\vec{J} \tag{2.1.23}$$

2.2 Lens equation

We can see in Fig.2.1 the most basic GL setup which illustrates the impact of a deflecting mass on a light path. We can see that a "point mass" L is far from the "source" S by a distance D_{ds}. The lens mass is at distance D_d from the observer O. The source is at distance D_s, where $D_s = D_{ds} + D_d$, from the observer and its angular separation from the lens, is β. A light ray coming from the source passes through the lens at a distance J and is deflected by $\hat{\alpha}$ where the image of the source would be seen at angle θ.

Thus we can see from the geometry of Fig. 2.1 for a weak lens approximation where the angles are small that the lens equation is

$$\beta = \theta - \hat{\alpha}D, \tag{2.2.1}$$

where $D = \frac{D_{ds}}{D_s}$, and the impact parameter is

$$J = D_d\theta,$$

The deflection angle then can take the form

$$\hat{\alpha} = \frac{4M}{\theta D_d} \tag{2.2.2}$$

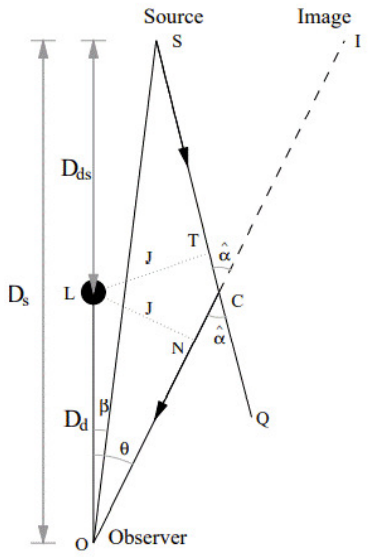

Figure 2.1: The lens diagram(O, L, and S represent the observer, deflector (lens), and source positions, respectively. The reference (optic) axis is denoted by OL. The angular separations of the source and image from the optic axis are β and θ. SQ and OI, which are tangents to the null geodesic at the source and observer positions, respectively; LN and LT, which are perpendiculars to these tangents from L and are called impact parameter. The Einstein bending angle is $\hat{\alpha}$. D_s stands for observer-source distance, D_{ds} for lens-source distance, and D_d stands for observer-lens distance.) (Virbhadra and Ellis, 2000)

2.3 Image positions

It is generally known that Schwarzschild black hole lensing produces two images one on the same side as the source from the optical axis called "Primary images" and we refer to it by "P", and another called "Secondary image" on the opposite side which we refer to it as "S".

These primary and secondary images are created because of the light deflection in a weak gravitational field without any looping of light rays around the lens Eiroa and Sendra (2011). Thus by inverting the lens equation (2.2.1), the angular positions of the primary (positive sign) and secondary images (negative sign) are

$$\theta_{p,s} = \frac{1}{2}\left(\beta \pm \sqrt{\beta^2 + 4\theta_E^2}\right), \tag{2.3.1}$$

where instead of two point pictures, an Einstein ring θ_E with angular radius E is obtained for perfect alignment when $\beta = 0$,

$$\theta_E = \sqrt{\frac{4DM}{D_d}}. \tag{2.3.2}$$

The Einstein ring is a very important tool to give us an approximate scale of the angular deflection we would expect from a given lens. We start using *Mathematica* and do our numerical computations to solve for lens equation and find the primary and secondary images. We then use our results to plot

different graphs to study how the angular position of the images would change with different values of the angular position of source β and D. We can see that as we fix the lens-observer distant $D_d = 7.62kpc$ the source-lens distance D_{ds} changes as D changes.

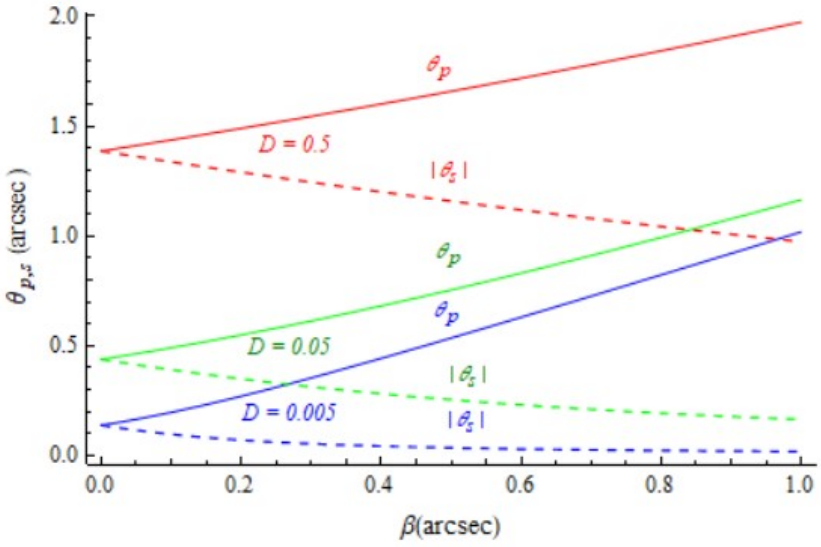

Figure 2.2: The angular positions of primary images θ_p and secondary image $|\theta_s|$ against the angular position of source β for different values of $D = 0.5$ (red), $D = 0.05$ (green), $D = 0.005$ (blue), where we consider the GL for MDO with mass $M = 3.61 \times 10^6 M_\odot$ and at distance $D_d = 7.62kpc$ from the observer so $M/D_d \approx 2.26 \times 10^{-11}$

We can see in Fig 2.2 that for a specific value of D the angular positions of primary θ_p and secondary $|\theta_s|$ images increases and decreases respectively as the angular position of source β increase. For different values of D, we can see that at a given value of β the angular positions of primary and secondary images increase. Thus the Einstein ring radius increases as the D value increases.

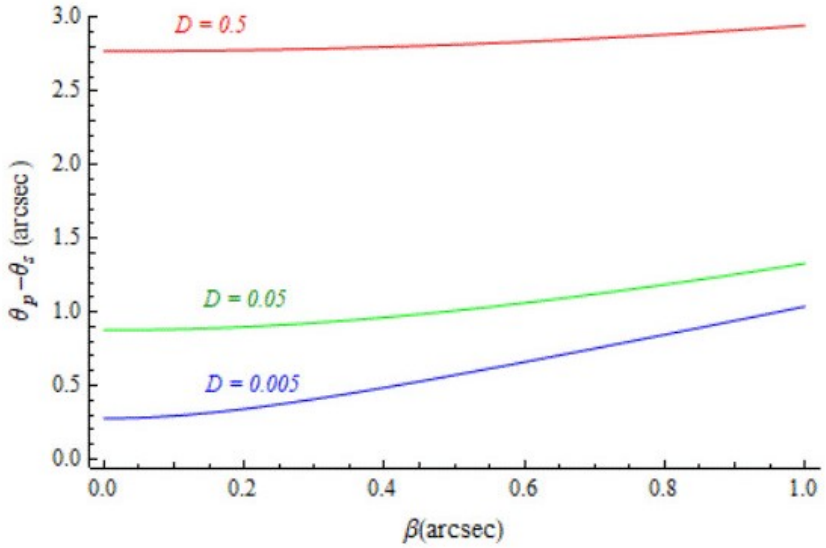

Figure 2.3: The angular separation $|\theta_p - \theta_s|$ between the primary images θ_p and secondary image $|\theta_s|$ against β for different values oof $D = 0.5$ (red), $D = 0.05$ (green), $D = 0.005$ (blue).

In Fig 2.3, we evaluate the angular separation between the primary and secondary images and we plot our results against the angular position of source β. The angular separation of two images increases as the values of the source angular position increase. For a given value of β, we can see that the angular separation increases as the value of D increases.

Now, we can demonstrate how the deflection angle varies for primary and secondary images, by using Eq. (2.3.1) and lens equation. The deflection angle as a function of θ and β can be written as

$$\hat{\alpha}(\beta,\theta) = \frac{1}{D}(\theta_{p,s} - \beta) \tag{2.3.3}$$

$$= \frac{1}{D}\left[\frac{1}{2}\left(\beta \pm \sqrt{\beta^2 + 4\theta_E^2}\right) - \beta\right] \tag{2.3.4}$$

We represent the dependence of deflection angle for primary and secondary images on angular position of source β and different values of D in Fig. 2.4

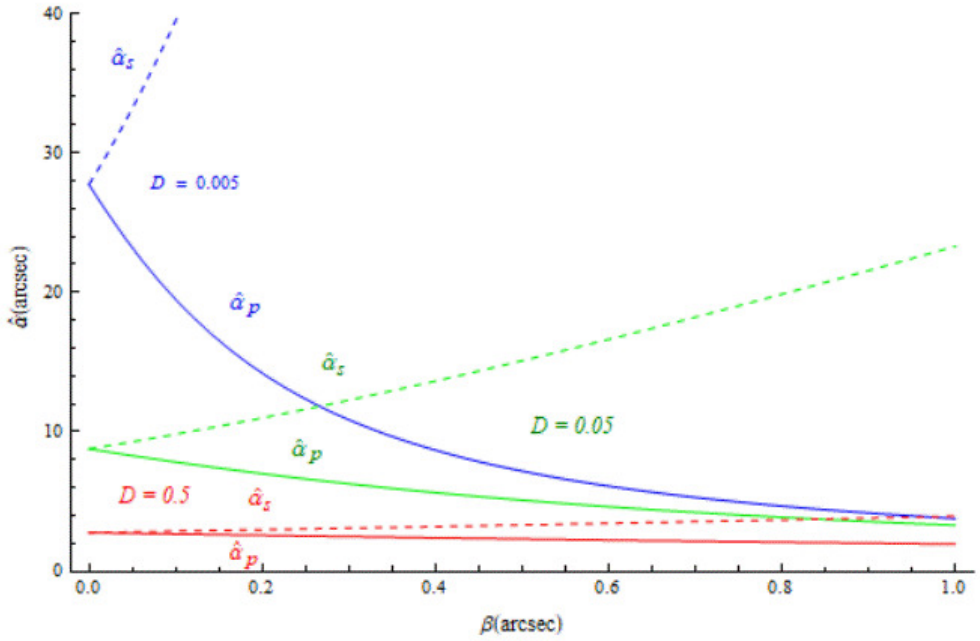

Figure 2.4: The deflection angle of primary image $\hat{\alpha}_p$ and secondary image $|\hat{\alpha}_s|$ against β for different values of $D = 0.5$ (red), $D = 0.05$ (green), $D = 0.005$ (blue), where we consider the GL for MDO with mass $M = 3.61 \times 10^6 M_\odot$ and at distance $D_d = 7.62kpc$ from the observer so $M/D_d \approx 2.26 \times 10^{-11}$.

It is evident that for a given value of D, the deflection angle increases for secondary image and decreases for primary image as β increases. However, for a given value of β, the deflection angle increases as D increases.

2.4 Magnifications

Light deflection has no effect on surface brightness. Without the lens, the surface brightness of the image is the same as the source. However, in a gravitational field, light deflection changes not only the direction of a light ray, but also the cross-section of a bundle of rays. Because the light deflection has no effect on the source's surface brightness, the apparent brightness of the source is magnified proportionally to the solid angle. Therefore, the ratio of the solid angle of an image to that of its corresponding source in the absence of the lens is the magnification,

$$\mu = \left|\frac{\sin\beta}{\sin\theta}\frac{d\beta}{d\theta}\right|^{-1} \approx \left|\frac{\beta}{\theta}\frac{d\beta}{d\theta}\right|, \tag{2.4.1}$$

where we can find by using eq. (2.3.1) the magnification of both primary and secondary images as follows

$$\mu_{p,s} = \frac{\beta^2 + 2\theta_E^2}{2\beta\sqrt{\beta^2 + 4\theta_E^2}} \pm \frac{1}{2}. \tag{2.4.2}$$

The total magnification in this case would be

$$\mu_{tot} = \mu_p + \mu_s = \frac{\beta^2 + 2\theta_E^2}{\beta\sqrt{\beta^2 + 4\theta_E^2}}. \tag{2.4.3}$$

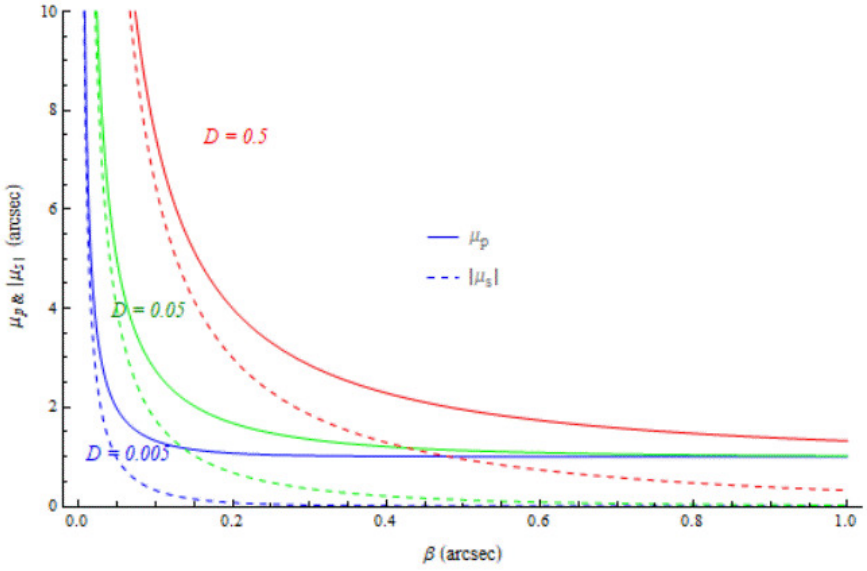

Figure 2.5: The magnification of primary image μ_p and secondary image $|\mu_s|$ against the angular position of source β for different values of $D = 0.5$ (red), $D = 0.05$ (green), $D = 0.005$ (blue), where we consider the GL for MDO with mass $M = 3.61 \times 10^6 M_\odot$ and at distance $D_d = 7.62kpc$ from the observer so $M/D_d \approx 2.26 \times 10^{-11}$

We find in Fig. 2.5, that the magnification of primary and secondary images decreases as β increases. Additionally, for different values of D and a given value of β the magnification of both images on

different sides of the optical axis increases as D increases.Thus, we can see that the magnification is inversely proportional to the source angular position β. It increases as the objects become more aligned $\beta \to 0$. Also, notice here that the total magnification will always be larger than unity even if $\beta/\theta_E \to \infty$.

If β is not close to O, the two images have very different brightness levels. The flux proportion is

$$\frac{\mu_p}{\mu_s} = \left(\frac{\sqrt{\beta^2 + 4\theta_E^2} + \beta}{\sqrt{\beta^2 + 4\theta_E^2} + \beta} \right)^2 . \tag{2.4.4}$$

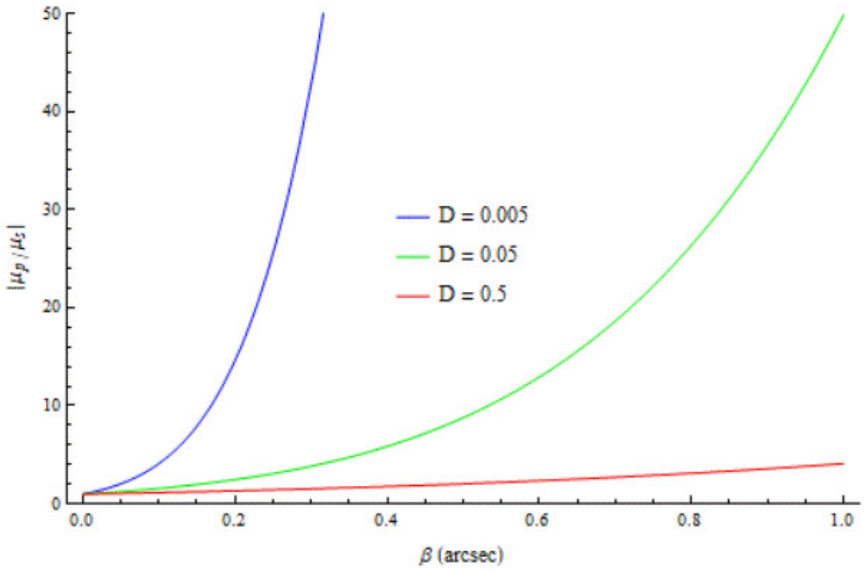

Figure 2.6: The ratio of magnification of the primary image to secondary image $|\mu_p/\mu_s|$ against the angular position of source β for different values of $D = 0.5, D = 0.05, D = 0.005$

As we can see in Fig. 2.6 the ratio of magnification of the primary image to the magnification of the secondary image increases as the angular position of the source increases. For a given value of β, we can also see how the ratio increases with different values of D. Accordingly, the magnification ratio and the image separation determine the Einstein angular radius θ_E and the angular distance of the source's "true" position β from the lens.

2.5 Strong limit

Many researchers have worked on the lensing theory in the strong field regime. In their groundbreaking works in the field, Darwin Brewer and Lewis (2005) and Atkinson predicted the occurrence of relativistic images. For the most part, Fritelli and Newman Frittelli and Newman (1999), Virbhadra and Ellis Virbhadra and Ellis (2000) , Bozza et al Bozza et al. (2001), and Perlick Perlick (2004b) developed the lens equation in the strong regime. After conducting a thorough numerical analysis of strong field lensing produced by Schwarzschild black hole, Virbhadra and Ellis Virbhadra (2009) first looked at the observational ramifications of the phenomenon when the galactic center's massive black hole serves as the lens. Considering the possibility that relativistic image detection may become feasible in the future and thus be used to test strong field gravity. Bozza et al.'s analytical method for determining the deflection angle in a strong field scenario demonstrated that the deflection angle diverges logarithmically as light rays get closer to the Schwarzschild black hole's photon sphere. Eiroa et al.Eiroa et al. (2002) expanded on this study to account for lensing brought on by Reissner-Nordstrom (RN) spacetime. Later, Bozza expanded the analytical lensing technique to a broader class of static spherically symmetric metrics and showed that such space-times frequently have the logarithmic divergence of the deflection angle at the photon sphere. Strong field lensing has been applied using Bozza's method to a number of intriguing cases, including lensing caused by the charged black hole of heterotic string theory Bhadra (2003), braneworld black holes Eiroa (2005), Einstein-Born-Infeld black holes Eiroa (2006), wormholes, and monopoles Perlick (2004a), among others. However, strong lensing has a wide range of applications in astronomy and cosmology. Studying the mass structure, formation, and evolution of elliptical galaxies, constraining the stellar initial mass function, and measuring cosmological parameters are some of the main applications. The weak field limit holds for most gravitational lenses in the universe. However, black holes and neutron stars are examples of compact objects that can act as gravitational lenses. In these cases, the weak field limit fails because photons pass through strong gravitational fields. The study of GL by a static compact lens is covered in the sections that follow. Thus, for a generic spherically symmetrical, and static metric, the line element is

$$\mathrm{d}s^2 = A(R)\mathrm{d}t^2 - B(R)\mathrm{d}R^2 - C(R)(\mathrm{d}\theta^2 + \sin^2\theta \mathrm{d}\phi^2) \tag{2.5.1}$$

The geodesic of the light ray must be integrated in order to find the deflection angle, which provides physical information about the lens. Thus, the deflection angle integral expression is

$$\hat{\alpha} = 2\int_{r_0}^{\infty} J\sqrt{\frac{B(r)}{C(r)[C(r)/A(r) - J^2]}}\mathrm{d}r - \pi \tag{2.5.2}$$

where J is the impact parameter, and r_0 is the shortest distance of the deflected photon from the deflector (lens). It can be defined as

$$J^2 = \frac{C(r_0)}{A(r_0)}. \tag{2.5.3}$$

In Schwarzchild metric,

$$A(r) = 1 - \frac{2GM}{rc^2},$$
$$B(r) = A(r)^{-1},$$

and

$$C(r) = r^2.$$

In the weak limit ($r_0 > 2GM/c^2$), the deflection angle reduces to

$$\hat{\alpha} = \frac{4GM}{c^2 J}. \tag{2.5.4}$$

After plugging $A(r), B(r)$ and $C(r)$ for Schwarzchild in Eq. (2.5.2) the deflection angle is given by

$$\hat{\alpha}(r_0) = 2\int_{r_0}^{\infty} \frac{dr}{r\sqrt{\left(\frac{r}{r_0}\right)^2\left(1-\frac{2M}{r_0}\right)-\left(1-\frac{2M}{r}\right)}}, -\pi \tag{2.5.5}$$

where the impact parameter in Eq. (2.5.3) is

$$J = r_0\left(1-\frac{2M}{r_0}\right)^{-\frac{1}{2}} \tag{2.5.6}$$

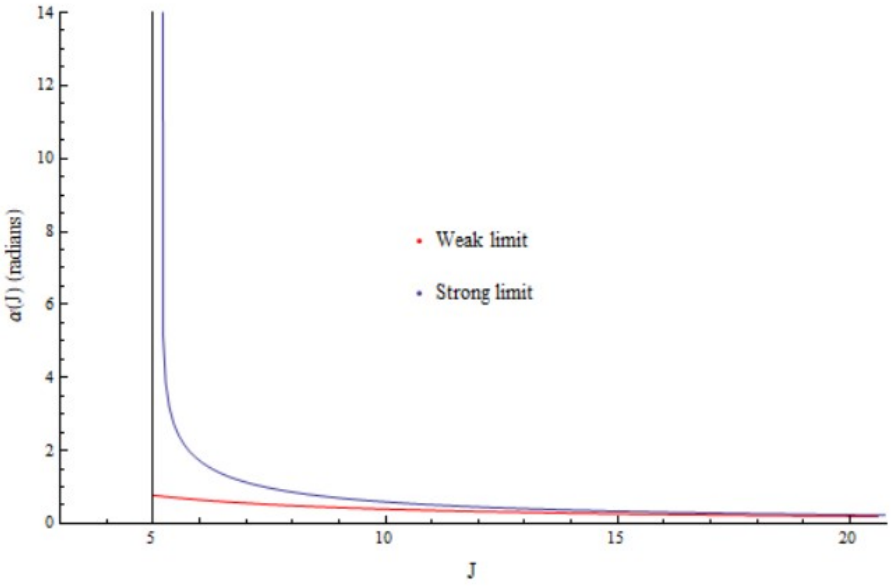

Figure 2.7: The deflection angle $\hat{\alpha}$ as a function of photon impact parameter, in radians, in strong limit Eq. (2.5.5) and weak limit Eq. (2.5.4)

We show in Fig. 2.7 how the deflection angle depends on the impact parameter J.The exact (strong limit) and approximate (weak limit) solutions to the geodesic equations for a Schwarzschild metric are displayed. The exact solution diverges for the impact parameter, as shown by the vertical line, indicating that the photon keeps looping.The deflection increases as the light ray trajectory approach the lens. At some impact parameter, $\hat{\alpha}$ becomes higher than 2π, causing the light ray to loop completely around the black hole. The light ray winds several times before emerging, further decreasing the impact parameter. This area or region of space where gravity is very strong that it forces photons to orbit the compact

object several times is called a photon sphere. For a Schwarzschild black hole, the radius of the photon sphere, which is also the lower bound for any stable orbit, is 1.5 times the Schwarzschild radius.

Using the Schwarzschild radius $2M$ (where $G = c = 1$) to define a dimensionless radial distance by

$$x = \frac{r}{2M}, \qquad x_0 = \frac{r_0}{2M}.$$

Then, the deflection angle is given by

$$\hat{\alpha}(x_0) = 2\int_{x_0}^{\infty} \frac{dx}{x\sqrt{\left(\frac{x}{x_0}\right)^2\left(1-\frac{1}{x_0}\right)-\left(1-\frac{1}{x}\right)}} - \pi, \tag{2.5.7}$$

where impact parameter yields

$$J = 2Mx_0\left(1-\frac{1}{x_0}\right)^{-\frac{1}{2}} \tag{2.5.8}$$

The first derivative of the deflection angle with respect to θ is required for calculations of image magnifications, thus

$$\frac{d\hat{\alpha}}{d\theta} = \hat{\alpha}'(x_0)\frac{dx_0}{d\theta}, \tag{2.5.9}$$

where the first and second factors on the right side of this equation are given by

$$\frac{dx_0}{d\theta} = \frac{x_0\left(1-\frac{1}{x_0}\right)^{\frac{3}{2}}\sqrt{1-\left(\frac{2M}{D_d}\right)^2 x_0\left(1-\frac{1}{x_0}\right)^{-1}}}{\frac{M}{D_d}(2x_0-3)} \tag{2.5.10}$$

and

$$\hat{\alpha}'(x_0) = \frac{3-2x_0}{x_0^2\left(1-\frac{1}{x_0}\right)}\int_{x_0}^{\infty} \frac{(4x-3)dx}{(3-2x)^2 x\sqrt{\left(\frac{x}{x_0}\right)}\left(1-\frac{1}{x_0}\right)-(1-\frac{1}{x})}, \tag{2.5.11}$$

Where the prime denotes the first derivative with respect to x_0.

2.6 Lens equation

Many authors have used direct trigonometric relationships to produce results for weak lensing and strong lensing that are more accurate. The one provided by Virbhadra and Ellis Virbhadra and Ellis (2000) is one of the most helpful,

$$\tan|\theta| - \tan\beta - D[\tan|\theta| + \tan\alpha - |\theta|] = 0 \tag{2.6.1}$$

Even more generic lens equation have been developed in this Ref. Dąbrowski and Schunck (2000),

$$\sin\gamma = D\cos|\theta| cos[\arcsin(D\sin(|\theta| - \gamma)][\tan|\theta| + \tan(\alpha - |\theta|)], \tag{2.6.2}$$

where $\gamma = \theta - \beta$

One can compare the accuracy of the various lens equations and then select the simplest expression that is compatible with the available astrometric precision, presuming that observations of the lensed image positions are (or soon will be) capable of resolving angular differences on the order of microarcseconds Ref. Jin et al. (2008).

We will use the Virbhadra and Ellis gravitational lens equation (2.6.1) for our analysis. It allows for arbitrary large as well as small deflections of light. This equation assumes that the angular position of the light source is small and that the source as well as the observer are situated at great distances from the lens (deflector). (The first assumption has no negative effects on the lens equation's applicability; typically, GL is meaningful for small angular source positions.)

$$\tan\beta = \tan\theta - \frac{D_{ds}}{D_s}[\tan\theta + \tan(\hat{\alpha} - \theta)], \tag{2.6.3}$$

where the perpendicular distance between the lens's center of mass and the tangent to the null geodesic at the source position (impact parameter) is

$$\sin\theta = \frac{J}{D_d} \tag{2.6.4}$$

The symbols β and θ, which denote the angular positions of an unlensed source and images, respectively, are measured from the optical axis, which is the line connecting the observer and the gravitational lens's center of mass. These angles are given positive and negative signs, respectively, depending on whether they are measured clockwise or anticlockwise from the optical axis. $\hat{\alpha}$ denotes the total angle by which the light ray is bent while passing through the lens' gravitational field on its way from the source to the observer. Null geodesics that are bent inward or outward from the lens have $\hat{\alpha} > 0$ and $\hat{\alpha} < 0$, respectively. Observer-lens, lens-source, and observer-source angular diameter distances are denoted by the letters D_d, D_{ds}, and D_s. Mathematically, the values of parameter D fall between (0, 1). However, the value of D should not be taken too close to zero, though, in order for the lens equation to be valid.

2.7 Image position

If a lens is very compact, a light ray passing close to it will experience significant deflection and will thus loop around the lens once, twice, three times, or many times (depending on the closest distance of approach from the lens's center) before reaching the observer. Relativistic images are defined as those images that occur as a result of light deflections by angles greater than $\hat{\alpha}3\pi/2$. Similarly, for the angular source position $\beta = 0$, relativistic Einstein rings are defined as ringed-shaped images that can form as a result of light deflections by angles greater than $\hat{\alpha} > 2\pi$. Thus, relativistic Einstein rings are relativistic images in the case of $\beta = 0$.

Finally, when $J = (3\sqrt{3})/2$, hence $x_0 = 3/2$, the deflection angle diverges and the light ray is captured by the black hole. There is one specific value of the impact parameter for each loop we add to the light ray geodesic such that the observer is reached by the light coming from the source. As a result, there will be an infinite number of images on each side of the lens. The order of relativistic images on each side of the optical axis can be usefully defined. We assign order 1 to the most distant relativistic images on both sides of the optical axis, order 2 to the closest inner ones, and so on. Thus, the outermost relativistic Einstein ring has the order 1 according to this definition. Two infinite sets of point relativistic images are produced when $\beta \neq 0$Virbhadra (2009). The deflection angle can be approximated for high alignment by

$$\hat{\alpha} = \pm n\pi \pm \Delta\hat{\alpha}_n, \tag{2.7.1}$$

where with $n \in \mathbb{N}$ and is called the winding number, which has an even value for standard lensing. The plus and minus signs represent the relativistic images produced on the primary and secondary image sides, respectively. Thus, for high alignment, the lens equation is given by

$$\beta = \theta_n \mp D\Delta\hat{\alpha}_n. \tag{2.7.2}$$

We solve for θ and find θ as a function of deflection angle $\theta(\hat{\alpha})$,

$$\theta = \theta_{p,s}[1 + \mathrm{e}^{(\mathrm{c}_2 - \hat{\alpha})/\mathrm{c}_1}]. \tag{2.7.3}$$

The angular position of the n-th image is given by a first-order Taylor expansion around $\hat{\alpha} = n\pi$

$$\theta_n = \theta_n^0 \pm \xi_n\Delta\hat{\alpha}_n, \tag{2.7.4}$$

where $c_1 = 1$ and $c_2 = \ln\left[216(7 - 4\sqrt{3})\right] - \pi$ for Schwarzschild metric,

$$\theta_n^0 = \theta_{p,s}[1 + \mathrm{e}^{(\mathrm{c}_2 - \mathrm{n}\pi)/\mathrm{c}_1}], \tag{2.7.5}$$

and

$$\xi_n = \frac{\theta_{p,s}}{c_1}\mathrm{e}^{(\mathrm{c}_2 - \mathrm{n}\pi)/\mathrm{c}_1}. \tag{2.7.6}$$

Using Eq. (2.7.1), we find

$$\Delta\hat{\alpha}_n = \pm(\theta_n - \beta)/D, \tag{2.7.7}$$

Thus, the angular position can be written as

$$\theta_n = \left(1 \pm \frac{\xi_n}{D}\right)^{-1} \left(\theta_n^0 \pm \frac{\xi_n}{D}\beta\right), \tag{2.7.8}$$

where $D = D_{ds}/D_s$.

The angular positions of the images are finally determined by using that $0 < \xi_n/D < 1$ and only keeping the first order term in ξ_n/D,

$$\theta_n = \pm\theta_n^0 + \frac{\xi_n}{D}(\beta \mp \theta_n^0). \tag{2.7.9}$$

An endless series of Einstein rings With angular-radius

$$\theta_n^E = \left(1 - \frac{\xi_n}{D}\theta_n^0\right) \tag{2.7.10}$$

are produced instead of the two-point image sequences on different sides of the optical axis.

We show in Fig 2.8, the dependence of the angular position of relativistic images of the first order and second order of the images on the same side as the primary images, on the angular position of source β and different values of D. The relativistic image's angular positions are very insensitive to changes in the values of β and D.

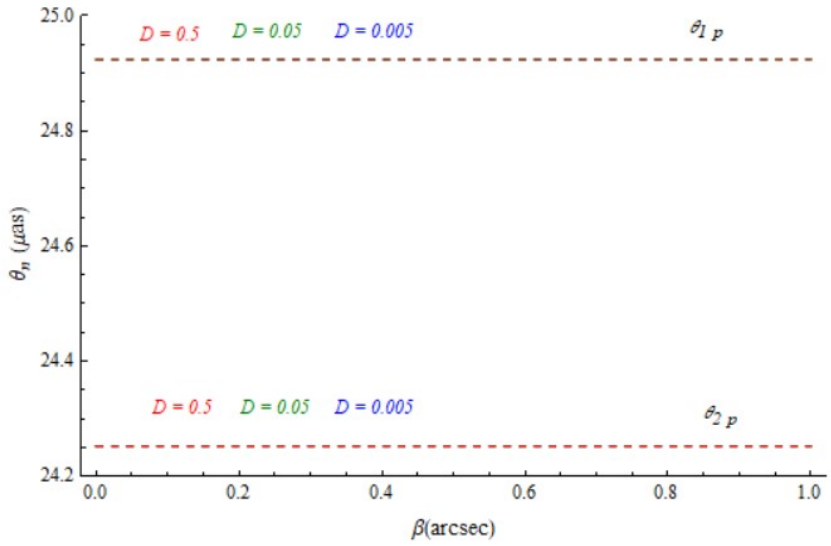

Figure 2.8: The angular position of relativistic images of order one θ_{1P} and order two θ_{2p} on the same side as primary images against angular position of the source β for different values of $D = 0.5$ (red), $D = 0.05$ (green), $D = 0.005$ (blue), where we consider the GL for MDO with mass $M = 3.61 \times 10^6 M_\odot$ and at distance $D_d = 7.62kpc$ from the observer so $M/D_d \approx 2.26 \times 10^{-11}$

We show in Fig 2.8, the dependence of the angular position of relativistic images of the first order and second order of the images on the same side as the primary images, on the angular position of source β and different values of D. The relativistic image's angular positions are very insensitive to changes in

the values of β and D. The angular positions of the first-order relativistic images on both sides of the optical axis are extremely close; however, $\theta_{1p} > |\theta_{1s}|$ for all values of β, with the exception at $\beta = 0$, where $\theta_{1p} = |\theta_{1s}|$. That is also the same case for any higher orders of images $\theta_{ns} \approx |\theta_{ns}|$. When $\beta = 0$ or a small value, θ_{1p} is greater when D is larger, but as β increases, there is a situation in which θ_{1p} is the same for all D values. It creates a critical angular source position at $\beta_{1c} \approx 24.9028\ microarcsec$ (μas), and for second-order relativistic images on the same side is $\beta_{2c} = 24.24$ (μas). We can also see that for angular separation in Fig. 2.9 that it is hard to see the changes for different values of D as the changes are very small.

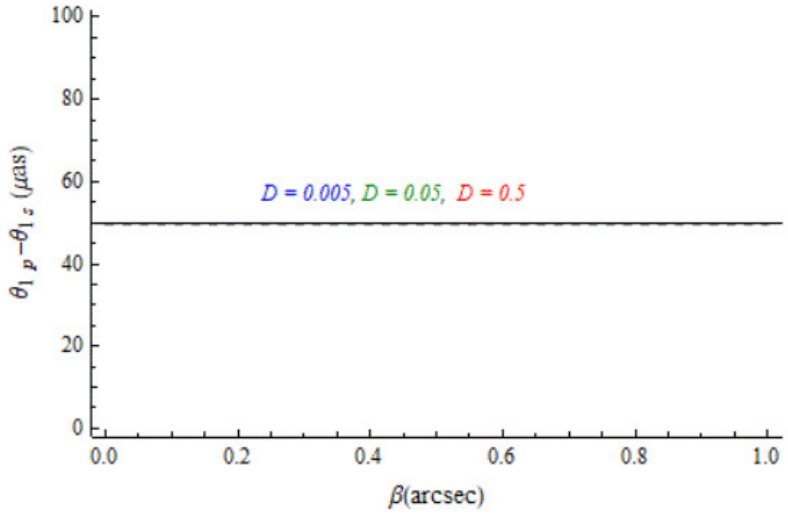

Figure 2.9: The angular separation between first order of angular position of relativistic images on the same side as primary image θ_{1p} and the first order of angular position of relativistic images on the same side as secondary image θ_{1s} against β for different values of $D = 0.5$ (red), $D = 0.05$ (green), $D = 0.005$ (blue).

In Fig 2.10, we show the angular separation between first and second order of the relativistic image $|\theta_{1p} - \theta_{2p}|$ on the same as the primary image. The angular separation is higher for lower value of D but for a large value of β. There exists a point where the values of $|\theta_{1p} - \theta_{2p}|$ for any two values of D are equal.

In Fig 2.11, We show here the angular separation between first and second order for the relativistic images on the same side as the secondary image. We notice here that the angular separations between the outermost two relativistic images (either on the primary or secondary image side) have just opposite qualitative dependence on $\beta$and D. $\theta_{1p} - \theta_{2p}$ increase with an increase in β (for a fixed D), but decreases with an increase in D (for a fixed β). $|\theta_{1s} - \theta_{2s}|$, on the other hand, decreases with an increase in β (for a fixed D), but increases with an increase in D (for a fixed β). The increase/decrease rate with change in the value of β (for a fixed D) is smaller as D increases. Variations in angular separations between relativistic images are extremely small in comparison to changes in β and D. For very small values of β, we conclude that angular separations between relativistic images are extremely insensitive to changes in the value of D.

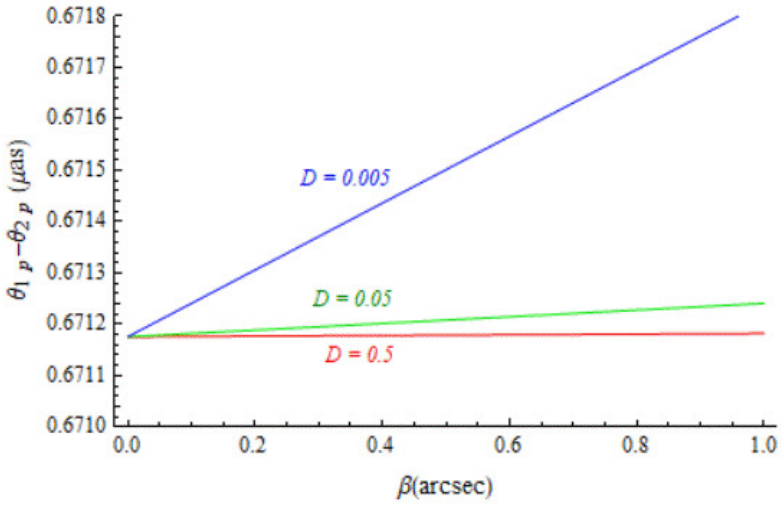

Figure 2.10: The angular separation between first order of angular position of relativistic images on the same side as primary image θ_{1p} and second order θ_{2p} of the same relativistic images against β for different values of $D = 0.5$ (red), $D = 0.05$ (green), $D = 0.005$ (blue).

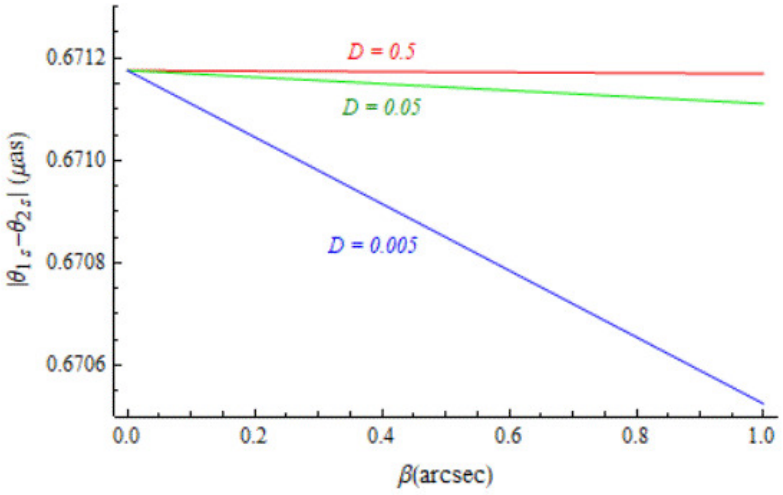

Figure 2.11: The angular separation between first order θ_{1s} and second order θ_{2s} of the angular position of relativistic images on the same side as secondary image against β for different values of $D = 0.5$ (red), $D = 0.05$ (green), $D = 0.005$ (blue).

2.8 Magnification:

Gravitational lensing conserves surface brightness Claudel et al. (2001) thus, magnification is defined as the ratio of the solid angles subtended by the θ_n-th image and the source.

$$\mu_n = \left| \frac{\sin\beta}{\sin\theta_n} \frac{d\beta}{d\theta_n} \right|^{-1} \tag{2.8.1}$$

The sign of an image's magnification indicates the image's parity. Critical curves (CCs) are singularities in the lens plane's magnification, and caustics are the corresponding values in the source plane. Images with a parity of 0 are referred to as critical images. Tangential and radial magnifications are defined as

$$\mu_t = \left(\frac{\sin\beta}{\sin\theta}\right)^{-1}, \tag{2.8.2}$$

$$\mu_r = \left(\frac{d\beta}{d\theta}\right)^{-1} \tag{2.8.3}$$

Singularities in these give tangential critical curves (TCCs) and radial critical curves (RCCs), respectively; corresponding values in the source plane are tangential caustics (TCs) and radial caustics (RCs). $\beta = 0$ represents the TC, and the corresponding values of θ are the TCCs. However, by using Eq. (2.7.9) we can write magnification as follows

$$\mu_n = \frac{1}{\beta}\left[\theta_n^0 + \frac{\xi_n}{D}(\beta - \theta_n^0)\right]\frac{\xi_n}{D} \tag{2.8.4}$$

and to first order in ξ_n/D, we have

$$\mu_n = \frac{1}{\beta}\frac{\theta_n^0\xi_n}{D}. \tag{2.8.5}$$

The outermost relativistic image is the brightest,(first order), and magnifications decrease exponentially as n increases. By adding the magnifications of both sets of relativistic images, the total magnification for a point source is obtained.

$$\mu = \frac{1}{\beta}\frac{8}{D_d^2 D c_1}\frac{e^{(c_2+\gamma)/c_1}[1 + e^{(c_2+\gamma)/c_1} + e^{2\pi/c_1}]}{e^{4\pi/c_1} - 1}, \tag{2.8.6}$$

magnifications are proportional to $1/D_d$. Then, unless β has values close to zero, i.e. almost perfect alignment, the relativistic images are very faint. An extended source analysis is required for $\beta = 0$, as the magnifications become infinite and the point source approximation fails.

In Fig, 2.12, we represent the dependence of magnification of first order of relativistic images that are on the same side as primary images on the angular position of source β. We notice for a given value of D, the magnification decreases as β increases. For a given value of β, the magnification increases as D decreases.

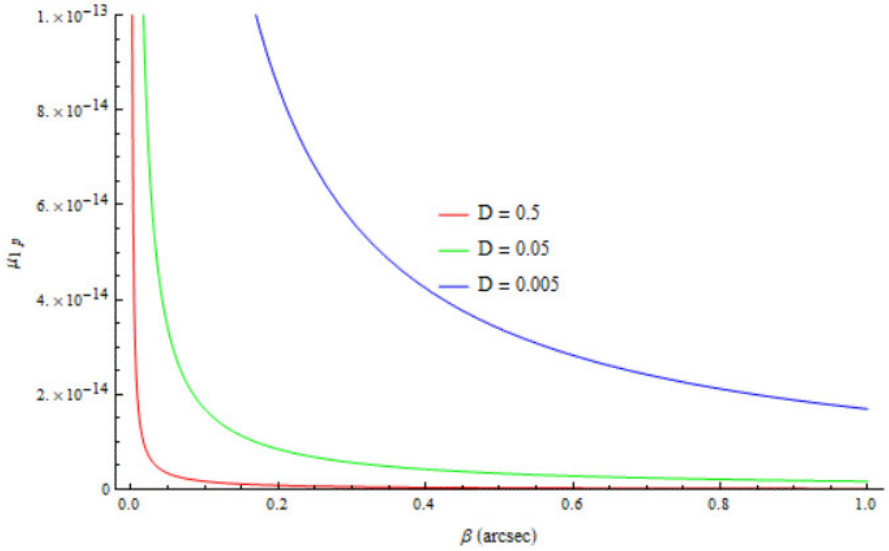

Figure 2.12: The magnification of first order of relativistic images on the same side as primary image μ_{1p} against β for different values of $D = 0.5, D = 0.05, D = 0.005$,

In Fig, 2.13, we represent the dependence of magnification of second-order for relativistic images that are on the same side as primary images, on the angular position of source β. We notice that values of magnification increase as β increases (D is fixed) but for fixed β value, decreases as D increases (Same for μ_{1p})

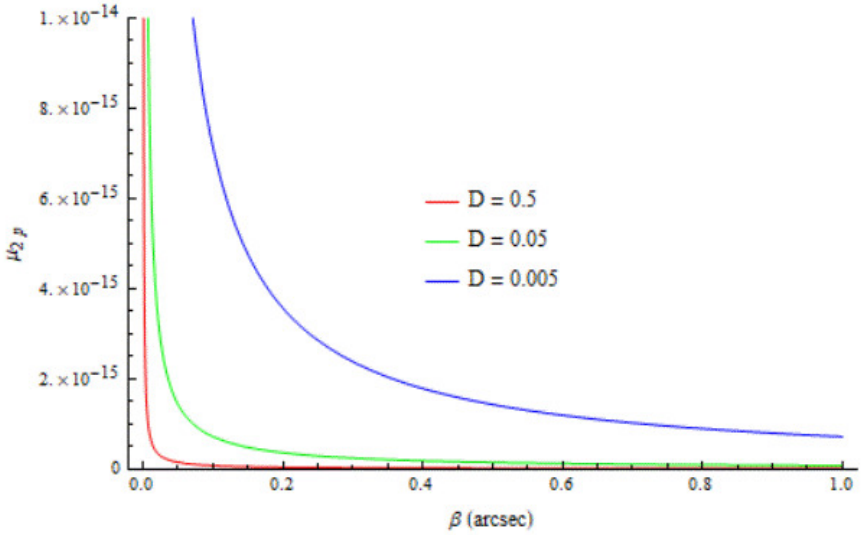

Figure 2.13: The magnification of second order of relativistic images on the same side as primary image μ_{2p} against β for different values of $D = 0.5, D = 0.05, D = 0.005$,

In Fig, 2.14, we show the dependence of the ratio of magnification of first order of relativistic images that are on the primary and secondary side, on the angular position of source β. For a given value of D, the ratio increases as β increases but for a fixed value of β, the ratio increases as D decreases.

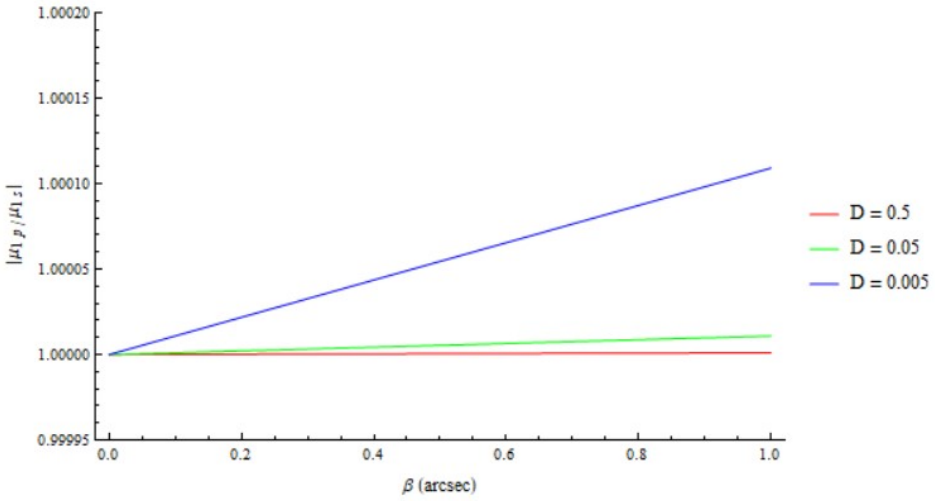

Figure 2.14: We plot here the ratio between magnification of the first order of relativistic images on the same side as primary image and first order of relativistic images on the same side as secondary image μ_{1p}/μ_{1s} against β for different values of $D = 0.5, D = 0.05, D = 0.005$,

In Fig, 2.15, we show the dependence of the ratio of magnification of first and second-order relativistic images that are on the primary side, on the angular position of source β and D. We notice that we have the same behavior as for the ratio between images on different sides μ_{1p}/μ_{1s}. We conclude that the magnification ratios of Relativistic images are much less sensitive to changes in the β and D. However, there are two significant differences between magnifications of primary-secondary pairs and relativistic images. First, With increasing angular source position β, the magnifications of relativistic images decrease much faster than those of primary and secondary images. Secondly, unlike primary and secondary images, the absolute magnifications of relativistic images increase as the value of D decreases for a fixed value of β. As a result, it would be easier to observe relativistic images of sources that are closer to the lens.

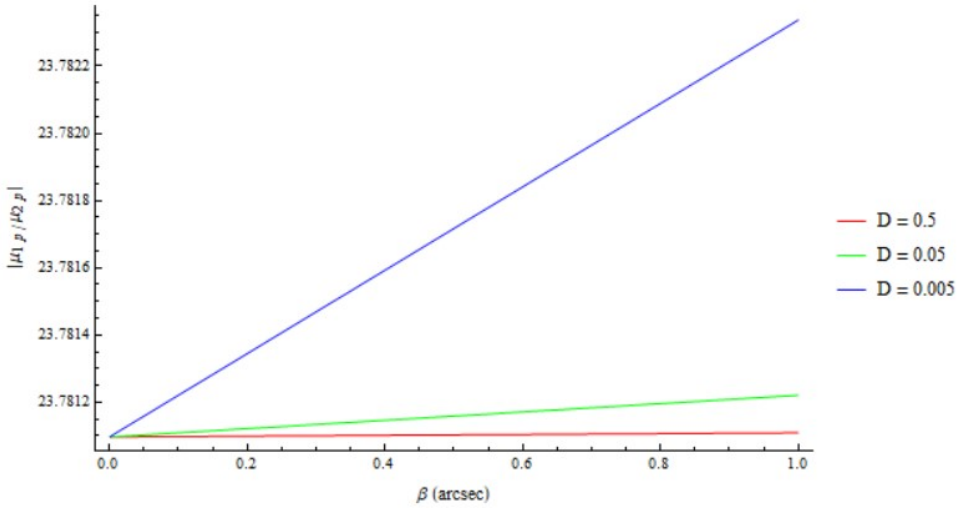

Figure 2.15: The ratio between magnification of first order μ_{1p} and second order μ_{1p}/μ_{2p} of relativistic images on the same side as primary image against β for different values of $D = 0.5$ (red), $D = 0.05$ (green), $D = 0.005$ (blue).

2.9 Time delay:

We take into account how light travels through a static, spherically symmetric space-time that is defined by the line element in eq (2.1.14). The amount by which light is delayed during propagation in the presence of a lens relative to an undeflected light ray is defined as the time delayVirbhadra and Keeton (2008). We find first the time required for light to travel from r to $r0$ (or opposite) that is expressed by

$$t(r, r_0) = t(r_0, r) = \int_{r_0}^{r} \sqrt{\frac{A(r)/B(r)}{1 - (\frac{r_0}{r})^2 \frac{B(r)}{B(r_0)}}} dr. \tag{2.9.1}$$

The time delay $\tau(x_0)$ of light traveling from the source to the observer with the closest of approach x_0 is defined as the difference between the light travel time for the actual ray in the gravitational field of the lens (deflector) and the travel time for the straight path between the source and the observer if there were no gravitational fields. Thus, by using the geometry of lens diagram we can obtain the following expression for time delay

$$\tau(x_0) = 2M \left[\int_{x_0}^{\chi_s} \frac{dx}{f(x)} + \int_{x_0}^{\chi_0} \frac{dx}{f(x)} \right] - D_s \sec\beta. \tag{2.9.2}$$

where

$$\chi_s = \frac{D_s}{2M} \sqrt{\left(\frac{D_{ds}}{D_s} + \tan^2\beta \right)} \tag{2.9.3}$$

$$\chi_0 = \frac{D_d}{2M}, \tag{2.9.4}$$

and

$$f(x) = \sqrt{\left(1 - \frac{1}{x}\right)^2 - \left(\frac{x_0}{x}\right)^2 \left(1 - \frac{1}{x}\right)^3 \left(1 - \frac{1}{x_0}\right)^{-1}} \tag{2.9.5}$$

The first and second terms in Eq. (2.9.2) give the travel time of light from the source to the point of closest approach and from that point to the observer, respectively. The final term gives the time it takes for light to travel from the source to the observer in the absence of a gravitational field. To see how the time delay function behaves for a light ray traveling in a weak gravitational field far away from the lens, we perform some analytical calculations using the method described in Keeton and Petters (2005). For images with large impact parameters, we obtain the time delay. The time delay is given by

$$\tau(\theta, \beta) = \frac{1}{2}\frac{D_d}{D}\left[\theta_E^2 + \beta^2 - \theta^2 - \ln\left(\frac{\theta^2 D_d}{4D_{ds}}\right)\right], \tag{2.9.6}$$

for given angular positions of the source β and image θ. The photons that create the primary and secondary images take different paths, and the time difference between them can be written as

$$\Delta\tau_{p,s} = 4M\left(\frac{-\beta\sqrt{\beta^2 + a\theta_E^2}}{2\theta_E^2} + \ln\left|\frac{\beta - \sqrt{\beta^2 + 4\theta_E^2}}{\beta + \sqrt{\beta^2 + 4\theta_E^2}}\right|\right), \tag{2.9.7}$$

where the redshift is taken to be 1. There is no time delay for perfect alignment when $\beta = 0$ because an Einstein ring is obtained. Large time delays can be obtained if $\beta/\theta_E > 1$, but the primary image magnification is close to one and the secondary image is very faint in this case. In the case of transient sources, the time delay between images can be a useful observable quantity. The ideal situation for a variable source is when β/θ_E is small enough to have large magnifications of both images, but not so close to zero that the time delay is longer than the source's typical time scale.

3. Gravitational lensing in scalar-tensor theories

3.1 $f(R)$ theories

In order to generalize the general theory of relativity, one or more of its underlying assumptions must be abandoned. Scalar-tensor theories, which hold that the gravitational field is composed of a scalar field in addition to the metric field, is one of the most significant extended theories of gravity (ETGs). We can still refer to it as a metric theory even though the scalar field is not related to the metric. Free particles follow geodesics because the scalar field only contributes to the production of the gravitational field and matter only reacts to the metric. Another intriguing family of ETGs is one in which curvature invariants are thought to influence how gravitational action is modified. One interesting case is the so-called $f(R)$ theories, which consider the Lagrangian as a generic function of scalar curvature,

$$S = \int d^4x\sqrt{-g}f(R) + S^{(m)}, \tag{3.1.1}$$

where R is the Ricci curvature scalar, det $g_{\mu\nu} = g$, and $S^{(m)}$is the standard matter Lagrangian. The action is then varied in accordance with the variational principle.

$$\delta S = \int d^4x[\delta\sqrt{-g}f(R) + \sqrt{-g}\delta f(R)] = 0, \tag{3.1.2}$$

The variation of $f(R)$ is

$$\delta f(R) = \frac{df}{dR}\delta R = f^{'}\delta R,$$

thus we need to evaluate

$$\delta R = R_{\mu\nu}\delta g^{\mu\nu} + g^{\mu\nu}\delta R^{\mu\nu}. \tag{3.1.3}$$

As we recall, when the Riemann tensor is contracted,

$$R^{\rho}_{\mu\lambda\nu} = \partial_\lambda\Gamma^{\rho}_{\nu\mu} + \Gamma^{\rho}_{\nu\mu}\Gamma^{\sigma}_{\nu\mu} - \partial_\nu\Gamma^{\rho}_{\lambda\mu} - \Gamma^{\rho}_{\nu\sigma}\Gamma^{\sigma}_{\lambda\mu}, \tag{3.1.4}$$

we can find the Ricci tensor

$$R_{\mu\nu} = R^{\lambda}_{\mu\lambda\nu}.$$

We must now change the connection with respect to the metric in order to find the variation of the Ricci tensor. Consider first a random alteration to the connection

$$\Gamma^{\rho}_{\nu\mu} \longrightarrow \Gamma^{\rho}_{\nu\mu} + \delta\Gamma^{\rho}_{\nu\mu}. \tag{3.1.5}$$

We can see that the difference between two connections is the variation of the connection. Consequently, we can take the covariant derivative of it snice it is also a tensor

$$\nabla_\lambda(\delta\Gamma^\rho_{\nu\mu}) = \partial_\lambda(\delta\Gamma^\rho_{\nu\mu}) + \Gamma^\rho_{\lambda\sigma}\delta\Gamma^\sigma_{\nu\mu} - \Gamma^\sigma_{\lambda\nu}\delta\Gamma^\rho_{\sigma\mu} - \Gamma^\sigma_{\lambda\mu}\delta\Gamma^\rho_{\nu\sigma}. \tag{3.1.6}$$

Thus, by varying the Riemann tensor we have

$$\delta R^\rho_{\mu\lambda\nu} = \partial_\lambda(\delta\Gamma^\rho_{\nu\mu}) + \delta\Gamma^\rho_{\lambda\sigma}\Gamma^\sigma_{\nu\mu} + \Gamma^\rho_{\lambda\sigma}\delta\Gamma^\sigma_{\nu\mu} - \partial_\nu(\delta\Gamma^\rho_{\lambda\mu}) - \delta\Gamma^\rho_{\nu\sigma}\Gamma^\sigma_{\lambda\mu} - \Gamma^\rho_{\nu\sigma}\delta\Gamma^\sigma_{\lambda\mu}. \tag{3.1.7}$$

We add and subtract this term $\Gamma^\sigma_{\lambda\nu}\delta\Gamma^\rho_{\sigma\mu}$, thus we find

$$\delta R^\rho_{\mu\lambda\nu} = \nabla_\lambda(\delta\Gamma^\rho_{\nu\mu}) - \nabla_\nu(\delta\Gamma^\rho_{\lambda\mu}). \tag{3.1.8}$$

Following contraction of the Riemann tensor, the Ricci tensor's variation is given by,

$$\delta R^\lambda_{\mu\lambda\nu} = \nabla_\lambda(\delta\Gamma^\lambda_{\nu\mu}) - \nabla_\nu(\delta\Gamma^\lambda_{\lambda\mu}). \tag{3.1.9}$$

We can now substitute in Eq. (3.1.3), thus

$$\delta R = R_{\mu\nu}\delta g^{\mu\nu} + g^{\mu\nu}[\nabla_\lambda(\delta\Gamma^\lambda_{\nu\mu}) - \nabla_\nu(\delta\Gamma^\lambda_{\lambda\mu})]. \tag{3.1.10}$$

The expression of $\delta\Gamma^\sigma_{\mu\nu}$ in terms of $\delta g_{\mu\nu}$ can be placed into Eq. (3.1.10)

$$\delta\Gamma^\sigma_{\mu\nu} = \frac{1}{2}g^{\sigma\lambda}(\nabla_\mu\delta g_{\lambda\nu} + \nabla_\nu\delta g_{\mu\lambda} - \nabla_\lambda\delta g_{\mu\nu}), \tag{3.1.11}$$

thus we have

$$\delta R = R_{\mu\nu}\delta g^{\mu\nu} + g^{\mu\nu}\left[\frac{1}{2}g^{\lambda\sigma}(\nabla_\lambda\nabla_\nu\delta g_{\sigma\mu} + \nabla_\lambda\nabla_\mu\delta g_{\sigma\nu} - \nabla_\lambda\nabla_\sigma\delta g_{\nu\mu} - \nabla_\nu\nabla_\lambda\delta g_{\sigma\mu} - \nabla_\nu\nabla_\mu\delta g_{\sigma\lambda} + \nabla_\nu\nabla_\sigma\delta g_{\lambda\mu})\right]. \tag{3.1.12}$$

We use $\delta g_{\mu\nu} = -g_{\mu\rho}g_{\nu\sigma}\delta g^{\sigma\rho}$ where we find

$$\delta R = R_{\mu\nu}\delta g^{\mu\nu} + \frac{1}{2}g^{\mu\nu}g^{\lambda\sigma}\nabla_\lambda\nabla_\mu g_{\sigma\rho}g_{\nu\beta}\delta g^{\rho\beta} - \frac{1}{2}g^{\mu\nu}g^{\lambda\sigma}\nabla_\lambda\nabla_\sigma g_{\mu\rho}g_{\nu\beta}\delta g^{\rho\beta} - \frac{1}{2}g^{\mu\nu}g^{\lambda\sigma}\nabla_\nu\nabla_\mu g_{\sigma\rho}g_{\lambda\beta}\delta g^{\rho\beta} + \frac{1}{2}g^{\mu\nu}g^{\lambda\sigma}\nabla_\nu\nabla_\sigma g_{\lambda\rho}g_{\mu\beta}\delta g^{\rho\beta}. \tag{3.1.13}$$

After relabeling a few dummy indices and applying the metric compatibility $\nabla_\rho g^{\mu\nu} = 0$, we can demonstrate that

$$\delta R = R_{\mu\nu}\delta g^{\mu\nu} + g_{\mu\nu}\Box\delta g^{\mu\nu} - \nabla_\mu\nabla_\nu\delta g^{\mu\nu} \quad , \tag{3.1.14}$$

where $\Box = g^{\mu\nu}\nabla_\mu\nabla_\nu$.

We will make use of the fact that for any matrix M

$$\ln(\det M) = \mathrm{Tr}(\ln M), \tag{3.1.15}$$

in order to find the term $\delta\sqrt{-g}$. Thus the variation of this identity is

$$\frac{1}{\det M}\delta(\det M) = \mathrm{Tr}\ (M^{-1}\delta M). \tag{3.1.16}$$

Since M^{-1} and δM might not commute, the cyclic property of trace was used in the previous equation. Next, we notice that $deltag$ variation is

$$\delta g = g(g^{\mu\nu}\delta g_{\mu\nu}), \tag{3.1.17}$$

and by using $\delta g_{\mu\nu} = -g_{\mu\rho}g_{\nu\sigma}\delta g^{\sigma\rho}$, we find

$$\delta g = g(-g^{\mu\nu}g_{\mu\rho}g_{\nu\sigma}\delta g^{\rho\sigma}) = g(-g_{\rho\sigma}\delta g^{\rho\sigma}). \tag{3.1.18}$$

Thus, we find

$$\delta\sqrt{-g} = -\frac{1}{2\sqrt{-g}}\delta g = \frac{1}{2}\frac{g}{\sqrt{-g}}g_{\mu\nu}\delta g^{\mu\nu}, \tag{3.1.19}$$

$$\delta\sqrt{-g} = -\frac{1}{2}\sqrt{-g}g_{\mu\nu}\delta g^{\mu\nu} \quad . \tag{3.1.20}$$

Next, we plug the equations (3.1.14) and (3.1.20) to the action which reduces to

$$\delta S = \int dx^4 \left[f(R)(-\frac{1}{2}\sqrt{-g}g_{\mu\nu}\delta g^{\mu\nu}) + \sqrt{-g}f^{'}(R)(R_{\mu\nu}\delta g^{\mu\nu} + g_{\mu\nu}\Box\delta g^{\mu\nu} - \nabla_\mu\nabla_\nu\delta g^{\mu\nu})\right], \tag{3.1.21}$$

$$\delta S = \int dx^4\sqrt{-g}\delta g^{\mu\nu}\left[-\frac{1}{2}f(R)g_{\mu\nu} + f^{'}(R)R_{\mu\nu} + g_{\mu\nu}\Box f^{'}(R) - \nabla_\mu\nabla_\nu f^{'}(R)\right]. \tag{3.1.22}$$

As a result the field equations of a generic $f(R)$ theory are

$$G_{\mu\nu} = R_{\mu\nu} - \frac{1}{2}Rg_{\mu\nu} \tag{3.1.23}$$

$$= \frac{1}{f^{'}(R)}\left[\frac{1}{2}g_{\mu\nu}\left(f(R) - f^{'}(R)R\right) - g_{\mu\nu}\Box f^{'}(R) + \nabla_{\mu}\nabla_{\nu}f^{'}(R)\right] + \frac{\tau^{(m)}_{\mu\nu}}{f^{'}(R)}, \tag{3.1.24}$$

Where $\tau^{(m)}_{\mu\nu}$ is the standard matter stress-energy tensor. These models are also known as fourth-order gravity since the two terms $g_{\mu\nu}\Box f^{'}(R)$ and $\nabla_{\mu}\nabla_{\nu}f^{'}(R)$ indicate fourth order derivatives of the metric g.

In the absence of ordinary matter $\tau^{(m)}_{\mu\nu} = 0$, the trace of field equations is

$$3\Box f^{'}(R) + Rf^{'}(R) - 2f(R) = 0, \tag{3.1.25}$$

and by combining the 00-component we find Capozziello and Faraoni (2010)

$$f^{'}(R)\left(3\frac{R_{00}}{g_{00}} - R\right) + \frac{1}{2f(R)} - 3\frac{\nabla_0\nabla_0 f^{'}(R)}{g_{00}} = 0, \tag{3.1.26}$$

which is of interest to us. It should be noted that $\nabla_0\nabla_0 f^{'}(R) = 1/2g^{ij}\partial_i g_{00}\partial_j f^{'}(R)$ is non-vanishing even if the metric is stationary such that $\partial_0 g_{\mu\nu} = 0$ This is because non-zero Christoffel symbols exist in the second covariant derivative. It should also be noted that Eq.(3.1.26) is universal and valid for any function $f(R)$.

3.2 $f(R) \propto R^n$

The most straightforward option for $f(R)$ is a power law with the form $f(R) \propto R^n$ (clearly, with n = 1, we recover the Einstein theory). We plug this form into our field equations Eq. (3.1.23)

$$k\tau_{\mu\nu} = (n-1)(2n-n)R^{n-1}\frac{\nabla_\mu R\nabla_\nu R}{R^2} - (n-1)nR^{n-1}\frac{\nabla_\mu\nabla_\nu R}{R} \tag{3.2.1}$$

$$+ nR^{n-1}R_{\mu\nu} - \frac{1}{2}g_{\mu\nu}RR^{n-1} - (n-1)(2n-n)g_\mu\frac{\nabla_\sigma R\nabla^\sigma R}{R^2} + (n-1)ng_{\mu\nu}R^{n-1}\frac{\Box R}{R}, \tag{3.2.2}$$

since we consider the vacuum case ($\tau_{\mu\nu} = 0$) we can write our field equations as follows

$$0 = -n\nabla_\mu R\nabla_\nu R - \nabla_\mu\nabla_\nu RR + \frac{1}{n-1}R_{\mu\nu}R^2 - \frac{1}{2(n-1)n}g_{\mu\nu}R^3 + ng_{\mu\nu}\nabla_\sigma R\nabla^\sigma R + g_{\mu\nu}(\Box R)R. \tag{3.2.3}$$

Any spherically symmetric solution of the vacuum field equations must be static and asymptotically flat, according to Birkhoff's theorem in general relativity. Therefore, we consider searching for spherically symmetric solutions, which we want to reduce to the Schwarzschild solution. We can write our solution as follows

$$ds^2 = -A(r)dt^2 + B(r)dr^2 + r^2d\Omega^2 \tag{3.2.4}$$

where $d\Omega^2 = d\theta^2 + \sin^2\theta d\phi^2$.

Thus, we can find from Eq. (3.1.26)

$$R_{00}(r) = \frac{2n-1}{6n}A(r)R(r) - \frac{n-1}{2B(r)}\frac{dA(r)}{dr}\frac{d\ln|R(r)|}{dr}. \tag{3.2.5}$$

Now, we can take the trace which can be written as follows

$$\Box R^{n-1}(r) = \frac{2-n}{3n}R^n(r) \tag{3.2.6}$$

We can notice that when $n = 1$, we have $R_{00} = 0$ and Eq. (3.2.6) reduces to $R = 0$, thus we can recover the Schwarzschild solution. Eqs. (3.2.5) and (3.2.6) become a system of two nonlinear coupled differential equations for the two functions $A(r)$ and $B(r)$ in general when R_{00} and R are expressed in terms of the metric (3.2.5).

Here, in accordance with Ref Capozziello et al. (2009), we offer a solution to the field equations in low-energy approximation. It is motivated to look for (Schwarzschild-like) solutions that have the following form.

$$A(r) = \frac{1}{B(r)} = 1 + \frac{2\Phi(r)}{c^2}, \tag{3.2.7}$$

Thus, the gravitational potential $\Phi(r)$ at distance r for a mass m is

$$\Phi(r, \sigma, r_c) = -\frac{GM}{2r}\left[1 + \left(\frac{r}{r_c}\right)^{\sigma}\right], \tag{3.2.8}$$

where σ is a strength parameter and r_c is a characteristic radius that is connected to one of the integration constants that must be chosen in order to solve the fourth-order theory differential equations. It is anticipated to be influenced by the unique characteristics of each system and can take different values depending on its mass and typical scale. It should be clear to see that the metric reduces to the Schwarzschild one and the Newtonian potential is recovered for $\sigma = 0$. The cases $\sigma > 1$ and $\sigma = 1$ (where the correction to the Newtonian potential asymptotically diverges and prevents asymptotic flatness, respectively) are not included. We need to find next the relation between σ and n. Thus, Eqs.(3.2.6) and (3.2.5) both simplify to algebraic equations when $\Phi(r)$ is introduced as follows

$$(n-1)(\sigma-3)\left[-\sigma(1+\sigma)V_1\frac{r}{r_c}^{(\sigma-3)}\right]^{n-1}\left[p_1 + \frac{r_c\sigma}{r}V_1 p_0\right] = 0, \tag{3.2.9}$$

where $V_1 = \frac{2GM}{c^2 r_c}$, and the two functions p_0 and p_1 equal to

$$p_0 = 3(\sigma-3)^2 n^3 - (5\sigma^2 - 31\sigma + 48)n^2 - (3\sigma^2 - 16\sigma + 17)n - (\sigma^2 - 4\sigma - 5),$$
$$p_1 = 3(\sigma-3)^2(1-\sigma)n^3 + (\sigma-3)^2(5\sigma-7)n^2 - (3\sigma^3 - 17\sigma^2 + 34\sigma - 36)n + (\sigma^2 - 3\sigma - 4)\sigma.$$

For particular values of n and σ, Eq. (3.2.9) is satisfied. Given that all $\sigma > 1$ result in divergences, then $\sigma = 3$ may be disregarded. Moreover, the fact that we assumed $R \neq 0$, then $n = 1$ is excluded. Only if $n > 1$ does the case $\sigma = -1$ provide a solution. We also rule out this value of σ because we are interested in a solution that is applicable regardless of what value n takes. Thus, we are left with the last factor that we need to solve in Eq. (3.2.9). Since both n and σ are of order unity, and $V_1 \ll 1$ for high scale-lengths r_c, then V_1 can also serve as a post-Newtonian parameter. Consequently, we can approximate the last factor in the post-Newtonian regime and find the algebraic equation

$$p_1(n, \sigma)\eta = 0, \tag{3.2.10}$$

which is an equation for σ as a function of n, where $\eta = r/r_c$, and it allows the following solutions

$$\sigma = \begin{cases} \frac{3n-4}{n-1} \\ \frac{12n^2-7n-1-\sqrt{p(n)}}{q(n)} \\ \frac{12n^2-7n-1+\sqrt{p(n)}}{q(n)} \end{cases}, \tag{3.2.11}$$

where

$$p(n) = 36n^4 + 12n^3 - 83n^3 + 50n + 1, \tag{3.2.12}$$
$$q(n) = 6n^2 - 4n + 2. \tag{3.2.13}$$

It is simple to verify that the second solution in Eq. (3.2.11), produces $\sigma = 0$ for $n = 1$, which reduces to the Newtonian potential as expected. The second solution is maintained in order to produce the

low-energy, far-field expression because the other two solutions do not satisfy this limit. Thus we can write the relation between n and correction parameter σ as follows

$$\sigma = \frac{12n^2 - 7n - 1 - \sqrt{36n^4 + 12n^3 - 83n^3 + 50n + 1}}{6n^2 - 4n + 2}, \tag{3.2.14}$$

where we present in the figure below how σ depends on n,

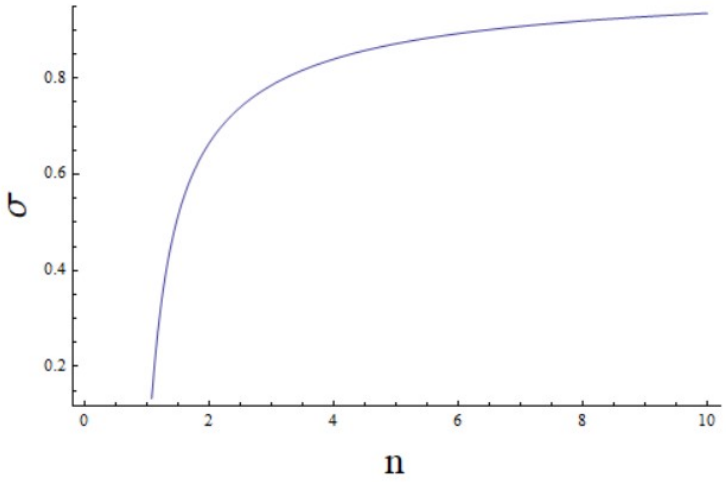

Figure 3.1: The correction parameter σ against n

It should be clear from Fig. 3.1 that the potential reduces to the Newtonian Φ_N in the case when $n = 1$ (implying that $\sigma = 0$) as expected, which is also true for the case of $r = r_c$. Gravity is weaker for smaller values of r, whereas it is stronger for values of $r > rc$, which is not the case in the Newtonian limit. The parameter r_c controls the scale at which deviations from the Newtonian potential occur, whereas the parameter σ controls the shape of the correction term. It is related to the fact that every $f(R)$ power-law model has a Noether symmetry, as demonstrated in Capozziello et al. (2007). It is a different gravitational radius from the Schwarzschild one from this standpoint, and it is dependent on the mass and size of the self-gravitating system. Thus r_c is not a universal parameter while the slope of the correction term σ is a universal quantity.

We can, in principle, set constraints on n using Eqs.(3.2.8) and (3.2.14) by imposing some physically motivated requirements on the modified gravitational potential. We need the potential to not diverge at infinity. With this in mind, we have

$$\lim_{r\to\infty} \Phi(r) = 0,$$

which impose a constrain on $\sigma - 1$ to be negative. Moreover, we can impose another condition by taking into account that the Newtonian potential $1/r$ is valid at Solar System scales, thus we must have $\sigma - 1 > -1$. This condition will assist in avoiding the increase in Φ at Solar System scales. Therefore, it is best to consider solutions within this range for σ

$$0 < \sigma < 1,$$

which gives $n > 1$ as a lower limit on the slope n of the gravity Lagrangian. We have selected a typical bulge radius of $r_c = 3240$ parsec (pc), which corresponds to an order of $10^{20}m$ Gergely (2021). As

a result, gravity outside r_{bulge} is stronger than in the Newtonian case, offering dark matter another possible source for a flat rotation curve.Capozziello et al. (2017)

3.3 Weak lensing

Since GR only makes its best predictions at the Solar System level, the debate over the short scale behavior of higher order gravity has recently become quite lively. In fact, measurements from weak field limit tests, such as the bending of light, the planets perihelion shift, and the frame dragging experiments, serve as indispensable checks for any theory of gravity. Since several classes of higher order theories of gravity are able to pass the standard Solar System tests, we believe that there are enough theoretical predictions to claim that they can be compatible with Newtonian and post-Newtonian regime [28]. However, there are several papers [Sotiriou (2005), Allemandi et al. (2005), Nojiri and Odintsov (2007), Chiba et al. (2007)] claiming that no progress has been made in the last forty years due to the fact that they approached the weak limit problem using various schemes and developing various parameterizations, where some of which occasionally proved to be incorrect [37, 38]. As a result, the discussion on the weak field limit of $f(R)$-theories is still far from being conclusive. The metric approach developed is the foundation for the current analysis.

3.4 Lens equation

In reference Capozziello et al. (2006), the weak lensing for point-like massive objects were investigated and we find that the deflection angle will be in this form for $0 < \sigma < 2$

$$\alpha = \frac{2GM}{c^2 J}\left[1 + \frac{\sqrt{\pi}(1-\sigma)\Gamma\left(1-\frac{\sigma}{2}\right)}{2\Gamma\left(\frac{3}{2}-\frac{\sigma}{2}\right)}\right]\left(\frac{J}{r_c}\right)^{\sigma}, \tag{3.4.1}$$

which is valid for $0 < \sigma < 2$ but as mentioned before because of the motivated physical constraints it is best to consider this narrowest range $0 < \sigma < 1$. The impact parameter is J, which in the weak limit can be written as $J = |\theta| D_d$. The deflection angle α reduces to the Schwarzschild angle in weak limit $\hat{\alpha}(J) = \frac{4GM}{c^2 J}$ when $\sigma = 0$ but for $\sigma = 1$ we have $\alpha = \hat{\alpha}(J)/2$. We study the behavior of the deflection angle between those limits by showing the dependence of deflection angle α on correction parameter σ for different values of J/r_c in the following figures.

In Figs 3.2 and 3.2 we can see that the deflection angle continuously decreases when the impact parameter is increased at any fixed value of σ, as in the Schwarzschild case. However, the rate at which α decreases with increasing J is slower for small impact parameters of order r_c. There is also a critical behavior at value $J/r_C = 2$. The deflection angle monotonically decreases with increasing σ below the critical value, and there is a single maximum at $\sigma_{\alpha_{max}}$ above it. The value of the correction parameter $\sigma_{\alpha_{max}}$ at maximum α increases as J/r_c increases.

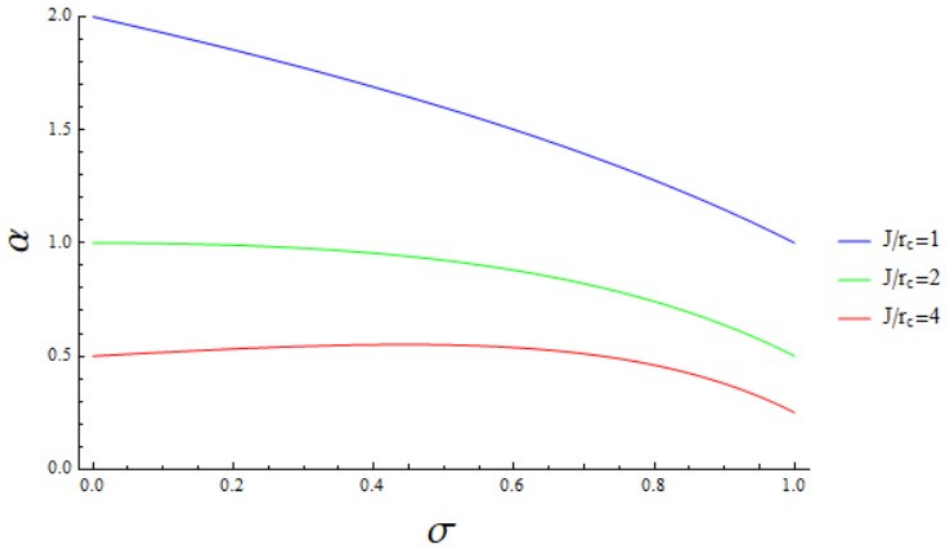

Figure 3.2: The dependence of defection angle α, in radians, on the the correction parameter σ for different values of $J/r_c = 1, J/r_c = 2, J/r_c = 4$, in units $GM/c^2 r_c = 1$, the critical behaviour appears at $J/r_c = 2$. We choose $r_c = 3240pc$

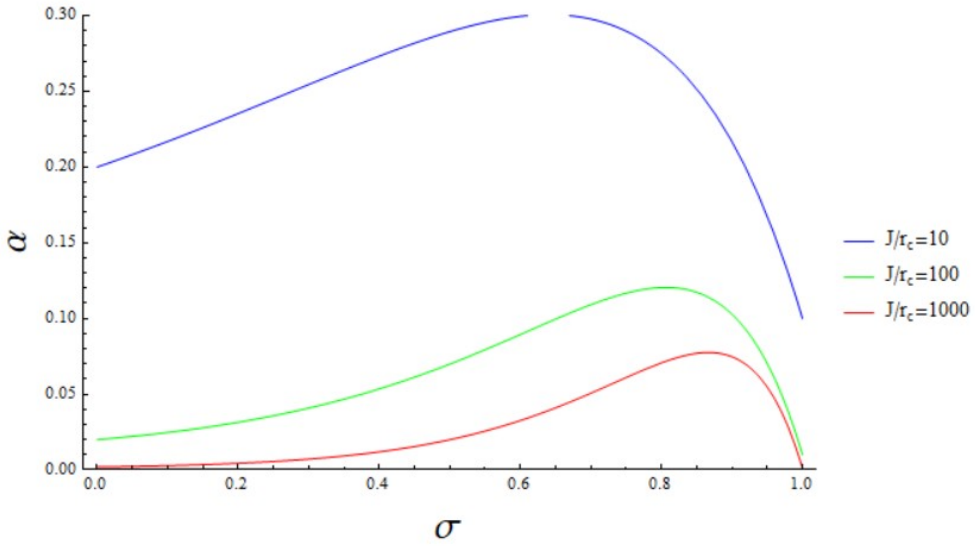

Figure 3.3: The dependence of defection angle α, in radians, on the the correction parameter σ for different values of $J/r_c = 10, J/r_c = 100, J/r_c = 1000$, in units $GM/c^2 r_c = 1$,We choose $r_c = 3240pc$

3.5 Images position

As we mentioned before, from the geometry of the lens diagram, one can see that images can either be positive (for the image on the right side of the optical axis called primary) or negative (for the image on the left side of the optical axis called secondary) at angles $\theta_{p,s}$ where $\alpha > 0$. Thus we can write the lens equation in the weak limit Capozziello et al. (2007) as follows

$$|\theta| - \beta - D\alpha = 0, \tag{3.5.1}$$

which indicates the position of the images $|\theta|$ (Primary and secondary) of the source.

3.6 Taking $f(R) = R^{1+\delta}$

The selection of the power-law of $f(R) \approx R^n$ action is important, which might seem unnatural when discussing deviations from GR. It is always possible to rewrite the $f(R)$ power-law function as $f(R) = R^{1+\delta}$, since n is any real number and large deviations from GR appear to be consistent with galactic dynamics. Thus, we are going to investigate the deflection of light by using one of the exact static and spherically symmetric solutions of $f(R) = R^{1+\delta}$. The static and spherically symmetric solution to the field equations is necessary in order to calculate the traditional tests of metric theories of gravity, such as the perihelion precession of Mercury and the bending and time-delay of light rays. To find such a solution, studies on this topic typically follow the recommended analysis for calculating the weak field geometry in GR; selecting a highly symmetric background, and determining the shape of spherically symmetric perturbations by linearising the field equations and solving them, to first-order in perturbations.

The exact spherically symmetric vacuum solution of $f(R) = R^{1+\delta}$ after finding the field equations (3.1.23) (as mentioned before for $f(R) = R^n$) for this form is given by the line-element.

$$ds^2 = -A(r)dt^2 + \frac{dr^2}{B(r)} + r^2 d\Omega, \tag{3.6.1}$$

Where

$$A(r) = r^{2\delta\frac{(1+2\delta)}{(1-\delta)}} + \frac{C}{r^{\frac{(1-4\delta)}{(1-\delta)}}} \tag{3.6.2}$$

$$B(r) = \frac{(1-\delta)^2}{(1-2\delta+4\delta^2)(1-2\delta(1+\delta))}\left(1 + \frac{C}{r^{\frac{(1-2\delta+4\delta^2)}{(1-\delta)}}}\right), \tag{3.6.3}$$

and C is a constant.

It should be clear to notice that when $\delta \to 0$. it reduces to the Schwarzschild solution. After a linear perturbation analysis is done for this solution as in ref Clifton (2006). The linearised version of the line element is

$$ds^2 = A_1(r)dt^2 + B_1(r)(dr^2 + r^2 d\Omega^2), \tag{3.6.4}$$

where

$$A_1(r) = r^{\frac{2\delta(1+2\delta)}{n}} \left(1 - \frac{(1-2\delta)C_1}{r^m}\right) \tag{3.6.5}$$

$$B_1(r) = r^{-2+\frac{2(1-\delta}{n})} \left(1 + \frac{C_1}{r^m}\right), \tag{3.6.6}$$

and

$$n^2 = (1 - 2\delta - 2\delta^2)(1 - 2\delta + 4\delta^2)$$
$$m^2 = \frac{(1 - 2\delta + 4\delta^2)}{(1 - 2\delta - 2\delta^2)},$$

Where C_1 is a constant.

Next, we find the geodesics equation for this metric and in the first order of δ, we have

$$\frac{d^2x}{dt^2} = -\frac{GM}{r^2}\left(1 + \left|\frac{dx}{dt}\right|^2\right) e_r + 4\frac{G^2M^2}{r^3}e_r + 4\frac{GM}{r^3}e_r + 4\frac{GM}{r_2}e_r.\frac{dx}{dt}\frac{dx}{dt} - \frac{\delta}{,}re_r, \tag{3.6.7}$$

where C_1 has been set using the Newtonian limit. We can notice there is a new term that completely vanishes when $\delta \to 0$. This term was used in [3] to impose the constraint on δ. It corresponds to a new force that diminishes as r^{-1}. The constraint appears from observations of the perihelion precession of Mercury and δ must have this value

$$\delta = 2.7,$$

which we are going to use to investigate the light deflection for this solution of $f(r)$. We will use the deflection angle equation in the weak limit which is given by

$$\alpha = \frac{r_c}{J}\left[1 + \frac{\sqrt{\pi}(1-\sigma)\Gamma\left(1 - \frac{\sigma}{2}\right)}{2\Gamma\left(\frac{3}{2} - \frac{\sigma}{2}\right)}\right]\left(\frac{J}{r_c}\right)^{\sigma}, \tag{3.6.8}$$

We show in Fig 3.4 how the deflection angle depends on the impact parameter J for $\delta = 2.7$, which gives us $\sigma = 0.827$.

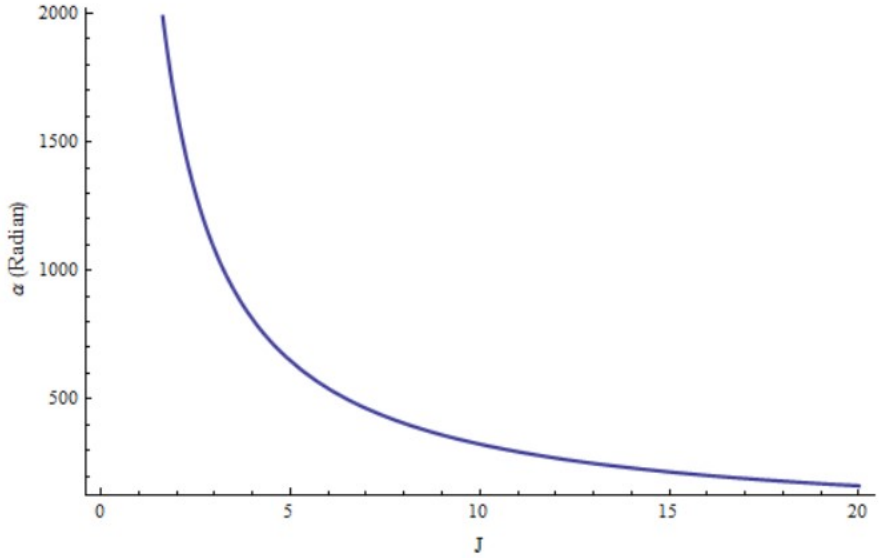

Figure 3.4: We show here the dependence of deflection angle α , in radians, on the impact parameter J for $\sigma = 0.827107$ and $r_c = 3240pc$

Thus we can notice for this value of δ, that the deflection angle decreases as the impact parameter J increases which is the same behavior as in GR. However, the values of the deflection angle, in radians, are larger than the values of the GR deflection angle in weak limit.

3.6.1 Image positions.

We solve numerically the lens equation (3.6.1) to find the dependence of deflection angle α on the angular position of source β for primary and secondary images. In Fig 3.5, we represent the dependence of the deflection angle on β for $\sigma = 0.827107$. We take into consideration the GL of MDO with $M = 3.61 \times 10^6 M_\odot$ as we did in the GR case. For a given value of β, we find that the deflection angle values decrease as D increases which is the same behavior as in GR. However, the curves are different for the different angular positions of images (Primary and Secondary). We notice that for a given value of D, the deflection angle of both images decreases as β increases which are different from our results in GR, where it decreases for the primary image and increases for the secondary image.

In Fig 3.5, we investigate the dependence of the angular position of primary and secondary images and angular separation between two images on β for different values of D. We find that, for a given value of D, the deflection angle for both images (primary and secondary) increases as $beta$ increases but this is not the case in GR, where α increases for the primary image and decreases for the secondary image. However, for a given value of β, the angular position of two images increases as D increases which is the same as GR. For angular separation between images, we can see that we have the same behavior as in GR where the angular separation between images increases as D and β increase.

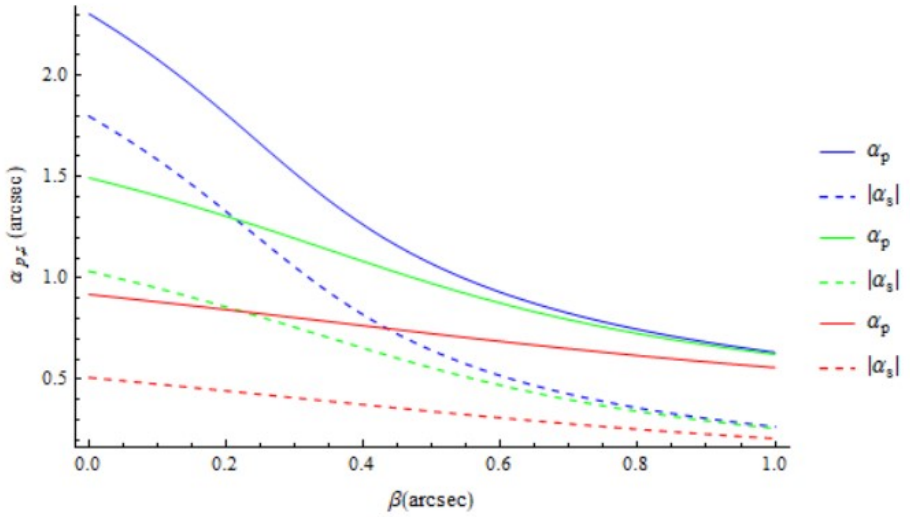

Figure 3.5: The dependence of the deflection angle $\alpha_{p,s}$ of primary and secondary images in $arcsec$ on β in $arcsec$, where we consider the GL for MDO with mass $M = 3.61 \times 10^6 M_\odot$ and at distance $D_d = 7.62kpc$ from the observer so $M/D_d \approx 2.26 \times 10^{-11}$ and $r_c = 3240pc$

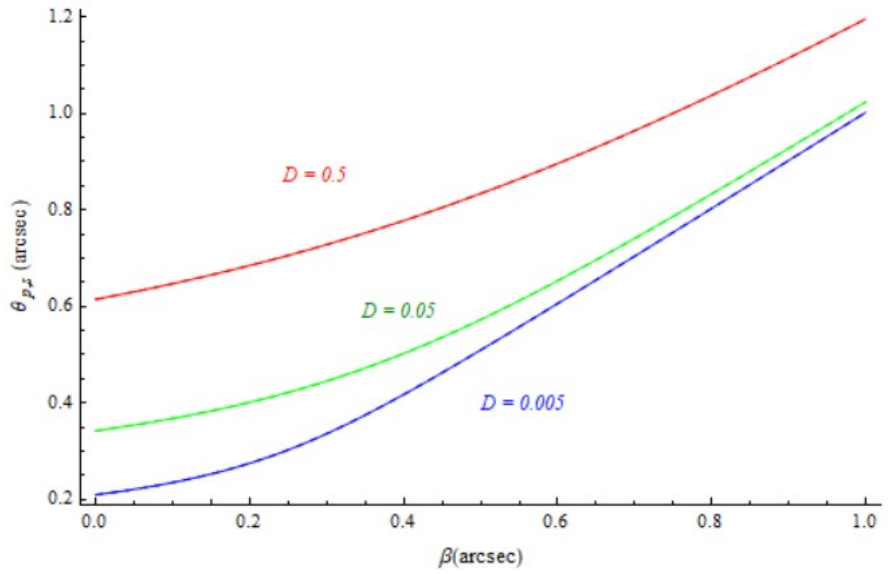

Figure 3.6: The angular position $\theta_{p,s}$ of primary and secondary images in $arcsec$ against $beta$ in $arcsec$, where we consider the GL for MDO with mass $M = 3.61 \times 10^6 M_\odot$ and at distance $D_d = 7.62kpc$ from the observer so $M/D_d \approx 2.26 \times 10^{-11}$, $r_c = 3240pc$ and $\sigma = 0.827107$

We notice in Figs (3.8), (3.9), (3.10), the difference between the GR and $f(R) = R^{1+\sigma}$ angular positions of images, angular separation of images and deflection angle in the weak limit of $\sigma = 2.7$. We notice that the values of deflection angle turned out to be very small in comparison with GR deflection angle. For angular positions and angular separations, we notice that the difference between the two theories is small and we have qualitatively the same behavior but $f(R)$ values are smaller than GR.

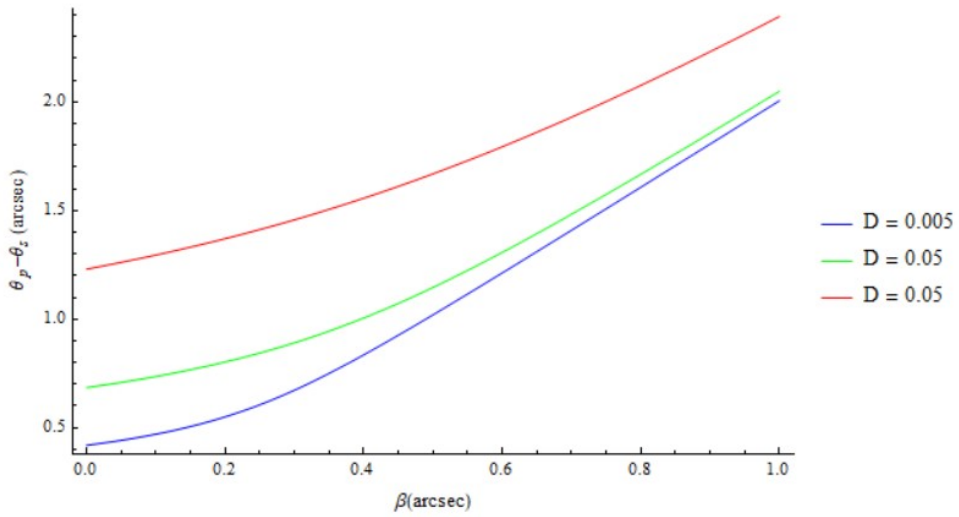

Figure 3.7: The angular separation $\theta_{p,s}$ between primary and secondary images in $arcsec$ against $beta$ in $arcsec$, where we consider the GL for MDO with mass $M = 3.61 \times 10^6 M_\odot$ and at distance $D_d = 7.62kpc$ from the observer so $M/D_d \approx 2.26 \times 10^{-11}$, $r_c = 3240pc$ and $\sigma = 0.827107$

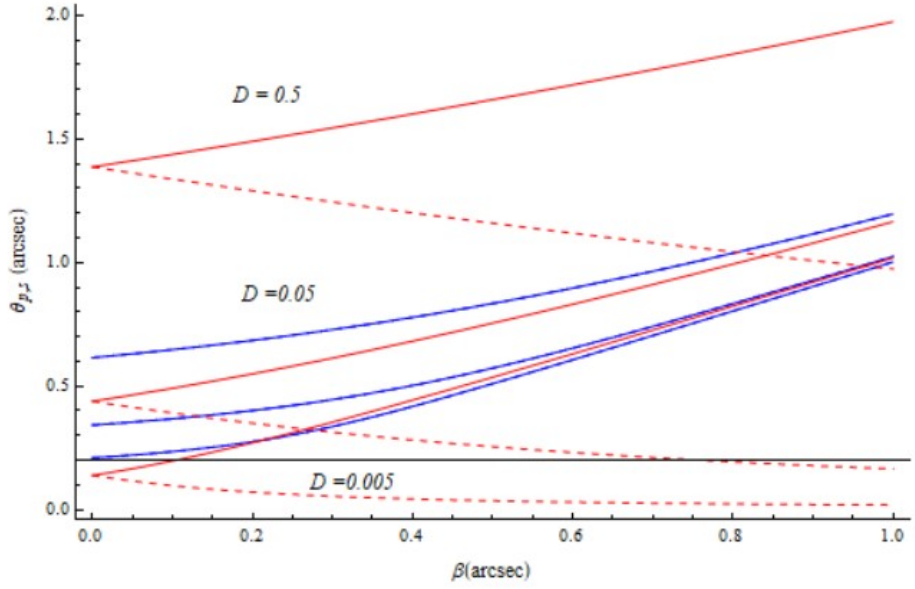

Figure 3.8: The angular position $\theta_{p,s}$ of primary and secondary images in both GR (Red) and $f(R)$ (blue) against $beta$ in $arcsec$ for different values of D. The dashed lines are the secondary images $|\theta_s|$ and continuous lines are primary images θ_p

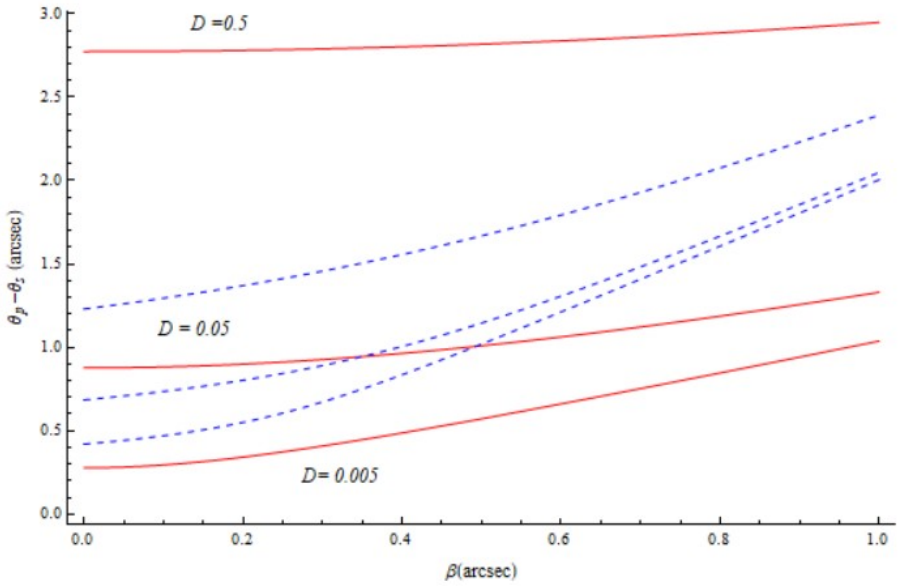

Figure 3.9: The angular separation $\theta_{p,s}$ between primary and secondary images in both GR (Red) and $f(R)$ (blue) against $beta$ in $arcsec$ for different values of D

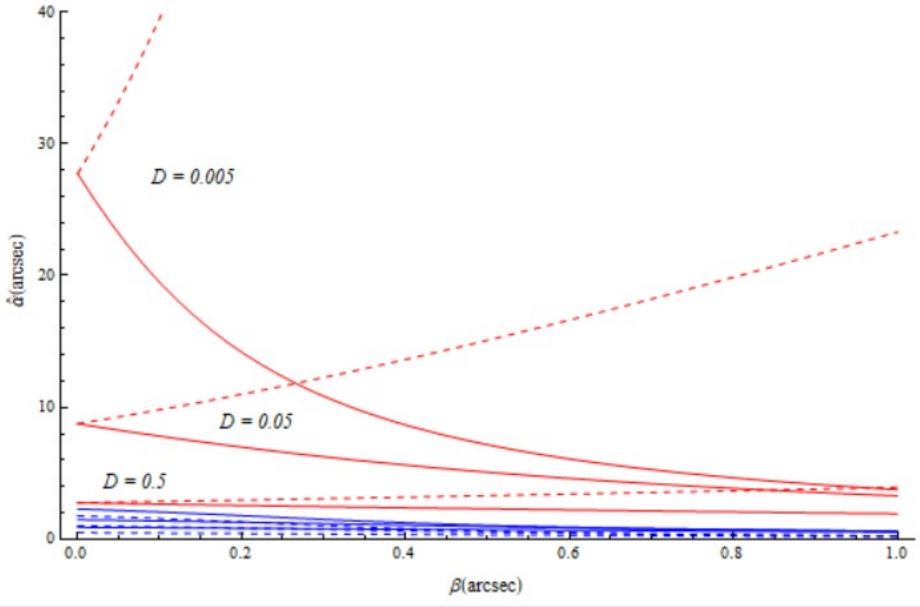

Figure 3.10: The deflection angle $\alpha_{p,s}$ of primary and secondary images iin both GR (Red) and $f(R)$ (blue) against β in $arcsec$ for different values of D. The dashed lines are the secondary images $|\theta_s|$ and continuous lines are primary images θ_p

4. Conclusions and prospects

As general relativity developed, gravitational lensing became an important method of measuring certain properties of gravitational fields. While the first observations of gravitational lensing were used to validate general relativity's theoretical predictions, it is now used to study the large-scale structure of the Universe, determine the behavior of compact stellar objects, and search for dark matter candidates. Gravitational lensing could be used to determine which of several gravitational theories is correct. It is well known that the predictions of bending angles obtained from Newtonian gravity differ by a factor of two from those obtained from Einstein's gravity. As a result, using gravitational lensing to investigate the differences between competing gravitational theories may provide a technique that can be used to determine the dimensionality of spacetime. As a result, we investigated the formalism of gravitational lensing in strong and weak limits. We revised all the analytical computations and results in accordance with the work done by modeling MDO of $M = 3.61 \times 10^6 M_\odot$ as a Schwarzchil black hole at the galactic center. We used Mathematica to solve equations numerically and to plot the results. We thoroughly reviewed the GL formalism for the weak limit. We drove the deflection angle before beginning to investigate the properties of various observables utilizing the lens equation. We discussed how, in the weak limit, the lens equation may be used to determine the image positions, magnifications and how, as a result, two-point images end up on opposite sides of the optical axis. We also discussed how we determine the image's magnification and how it varies as the angle of the source is changed. We demonstrated the deflection angle in strong limit and solved it numerically. In the strong limit, we reviewed the analytical computations for angular positions, magnifications, and time delay. We showed how the angular separation between the two outermost relativistic images (either on the main or secondary image side) has a qualitative dependence on β and D which is quite the opposite. The relativistic images have an angular position roughly equal to the angle subtended by the event horizon and are strongly demagnified, making their detection difficult. However, physical quantities measured for relativistic images would provide very accurate values for black hole masses and distances. We also showed how magnifications of primary and secondary images, as well as relativistic images, change as the values of β and D change. Images on the same side as the source and opposite side from the source have positive and negative magnifications and, as a result, positive and negative parities. We also showed the dependence of relativistic images magnification ratio on D and β. These magnification ratio measurements would yield very accurate values for D.

It was also interesting to look into gravitational lensing in theories other than Einstein's. There are several physical and mathematical reasons for these theories to expand General Relativity (GR). One of the reasons is our need to introduce unknown dark matter (DM) (to address dynamical phenomena such as the formation of self-gravitating astronomical structures) and dark energy (DE) (to address cosmic acceleration), in order to interpret recent observational data in the framework of GR. We discuss $f(R)$-gravity model. We start by driving the field equations and choose the power-law form of $f(R) = R^n$ as it is one of the simplest expressions for $f(R)$. We consider a spherically symmetrical solution in our analysis for gravitational lensing. We find that there is a characteristic radius r_c that appears as a constant of integration in order to solve for field equations. This constant depends on the scale and mass of the gravitational system. The deflection angle depends on the integral $I = (1/r)d\Phi/dr$. Thus, if we compare the potential of $f(R)$ and GR one, we find

$$\frac{\Phi(r)}{\Phi_{GR}(r)} = \frac{1}{2}\left[1 + \left(\frac{r}{r_c}\right)^\sigma\right]$$

,

$$\frac{I(r)}{I_{GR}(r)} = \frac{1}{2}\left[1 + (1-\sigma)\left(\frac{r}{r_c}\right)^{\sigma}\right]$$

so that

$$\Phi(r) > \Phi_{GR} r \Leftrightarrow r > r_c.$$

It should be clear to notice that on a galactic scale this condition where the $f(R)$ potential is larger than GR potential is met for typical values of r_c. Thus, there will be an increase in the rotation curve which is a good fit for observations without introducing dark matter. We also discussed the different properties of deflection of angle in $f(R)$ theory. We showed how it is dependent on the correction parameter σ that appears because of $f(R)$ potential. We also discussed the relation between that correction parameter and n. We demonstrated how the corrected deflection angle in weak limit is only valid for $0 < \sigma < 2$.

Finally, we chose a more particular form of power-law $f(R)$ theories, which is $f(R) = R^{1+\delta}$. Then we considered a physically symmetric solution in this case to investigate the gravitational lensing formalism in weak limit. We were able to find the deflection angle of primary and secondary images. We showed the dependence of the deflection angle on β and different values of D. It was concluded that the corrected deflection angle of this special case $R^{1+\delta}$ of $f(R)$ theories turned out to be lower than the classical GR deflection angle for the small angular position of the source $\beta < 1$. We also solved the deflection angle numerically to find the angular position $\theta_{p,s}$ for primary and secondary images. We showed how the angular position of primary and secondary images depends on the values of β and D. We noticed that the results turned out to be also lower than it is for primary and secondary images in GR. However, at a given value of β, the angular position would increase as D increases. This is qualitatively similar to the case of angular positions of primary and secondary images and the angular separation between them. As a future work, we would investigate the magnification and time delay in $f(R) = R^{1+\delta}$. We can also consider other spherically symmetric solutions for this form. It would be also intersecting to study gravitational formalism in strong field limit for this form of $f(R)$ and compare our results with the observational data.

Acknowledgements

I would like to express my deepest thanks and sincere graduate to my supervisor Dr. Alvaro de la Cruz-Dombriz, for his invaluable attention, guidance, and comments throughout the course of this project. It was a pleasure working with him.

I also express my deepest thanks to my mom and sister for their love and support, as well as my Gabe for his great support and understanding.

References

Allemandi, G., Francaviglia, M., Ruggiero, M. L., and Tartaglia, A. Post-newtonian parameters from alternative theories of gravity. *arXiv preprint gr-qc/0506123*, 2005.

Bhadra, A. Gravitational lensing by a charged black hole of string theory. *Physical Review D*, 67(10): 103009, 2003.

Bozza, V., Capozziello, S., Iovane, G., and Scarpetta, G. Strong field limit of black hole gravitational lensing. *General Relativity and Gravitation*, 33:1535–1548, 2001.

Brewer, B. J. and Lewis, G. F. When darwin met einstein: gravitational lens inversion with genetic algorithms. *Publications of the Astronomical Society of Australia*, 22(2):128–135, 2005.

Capozziello, S. and Faraoni, V. *Beyond Einstein gravity: A Survey of gravitational theories for cosmology and astrophysics*, volume 170. Springer Science & Business Media, 2010.

Capozziello, S., Cardone, V., and Troisi, A. Gravitational lensing in fourth order gravity. *Physical Review D*, 73(10):104019, 2006.

Capozziello, S., Stabile, A., and Troisi, A. Spherically symmetric solutions in f (r) gravity via the noether symmetry approach. *Classical and Quantum Gravity*, 24(8):2153, 2007.

Capozziello, S., Stabile, A., and Troisi, A. A general solution in the newtonian limit of f (r)-gravity. *Modern physics letters A*, 24(09):659–665, 2009.

Capozziello, S., Jovanović, P., Jovanović, V. B., and Borka, D. Addressing the missing matter problem in galaxies through a new fundamental gravitational radius. *Journal of Cosmology and Astroparticle Physics*, 2017(06):044, 2017.

Carroll, S. M. Lecture notes on general relativity. *arXiv preprint gr-qc/9712019*, 1997.

Carroll, S. M. and Traschen, J. Spacetime and geometry: An introduction to general relativity. *Physics Today*, 58(1):52, 2005.

Chiba, T., Smith, T. L., and Erickcek, A. L. Solar system constraints to general f (r) gravity. *Physical Review D*, 75(12):124014, 2007.

Claudel, C.-M., Virbhadra, K. S., and Ellis, G. F. The geometry of photon surfaces. *Journal of Mathematical Physics*, 42(2):818–838, 2001.

Clifton, T. Spherically symmetric solutions to fourth-order theories of gravity. *Classical and quantum gravity*, 23(24):7445, 2006.

Corda, C. The production of matter from curvature in a particular linearized high order theory of gravity and the longitudinal response function of interferometers. *Journal of Cosmology and Astroparticle Physics*, 2007(04):009, 2007.

Dąbrowski, M. P. and Schunck, F. E. Boson stars as gravitational lenses. *The Astrophysical Journal*, 535(1):316, 2000.

Doeleman, S., Agol, E., Backer, D., Baganoff, F., Bower, G. C., Broderick, A., Fabian, A., Fish, V., Gammie, C., Ho, P., et al. Imaging an event horizon: submm-vlbi of a super massive black hole. *arXiv preprint arXiv:0906.3899*, 2009.

Eiroa, E. F. Braneworld black hole gravitational lens: Strong field limit analysis. *Physical Review D*, 71 (8):083010, 2005.

Eiroa, E. F. Gravitational lensing by einstein-born-infeld black holes. *Physical Review D*, 73(4):043002, 2006.

Eiroa, E. F. and Sendra, C. M. Gravitational lensing by a regular black hole. *Classical and Quantum Gravity*, 28(8):085008, 2011.

Eiroa, E. F., Romero, G. E., and Torres, D. F. Reissner-nordström black hole lensing. *Physical Review D*, 66(2):024010, 2002.

Eisenhauer, F., Genzel, R., Alexander, T., Abuter, R., Paumard, T., Ott, T., Gilbert, A., Gillessen, S., Horrobin, M., Trippe, S., et al. Sinfoni in the galactic center: young stars and infrared flares in the central light-month. *The Astrophysical Journal*, 628(1):246, 2005.

Esposito-Farèse, G. Tests of scalar-tensor gravity. In *AIP conference proceedings*, volume 736, pages 35–52. American Institute of Physics, 2004.

Frittelli, S. and Newman, E. T. Exact universal gravitational lensing equation. *Physical Review D*, 59 (12):124001, 1999.

Gergely, L. Á. 26.1 deflection of light in schwarzschild geometry. *Modified Gravity and Cosmology: An Update by the CANTATA Network*, page 385, 2021.

Guo, G., Jiang, X., Wang, P., and Wu, H. Gravitational lensing by black holes with multiple photon spheres. *Physical Review D*, 105(12):124064, 2022.

Jin, W., Platais, I., and Perryman, M. A. *A Giant Step: From Milli-to Micro-Arcsecond Astrometry (IAU S248)*, volume 224. Cambridge University Press, 2008.

Keeton, C. R. and Petters, A. Formalism for testing theories of gravity using lensing by compact objects: Static, spherically symmetric case. *Physical Review D*, 72(10):104006, 2005.

LIGO. Ligo. Caltech-MIT, https://www.ligo.caltech.edu/, Accessed May 2018.

Lodge, O. J. Gravitation and light. *Nature*, 104(2614):354–354, 1919.

Meneghetti, M. *Introduction to Gravitational Lensing: With Python Examples*, volume 956. Springer Nature, 2021.

Nojiri, S. and Odintsov, S. D. Unifying inflation with λcdm epoch in modified f (r) gravity consistent with solar system tests. *Physics Letters B*, 657(4-5):238–245, 2007.

Perlick, V. Exact gravitational lens equation in spherically symmetric and static spacetimes. *Physical Review D*, 69(6):064017, 2004a.

Perlick, V. Gravitational lensing from a spacetime perspective. *Living reviews in relativity*, 7:1–117, 2004b.

Raychaudhuri, A. Relativistic cosmology. i. *Physical Review*, 98(4):1123, 1955.

Sotiriou, T. P. The nearly newtonian regime in non-linear theories of gravity. *arXiv preprint gr-qc/0507027*, 2005.

Sotiriou, T. P. f (r) gravity and scalar–tensor theory. *Classical and Quantum Gravity*, 23(17):5117, 2006.

Virbhadra, K. Relativistic images of schwarzschild black hole lensing. *Physical Review D*, 79(8):083004, 2009.

Virbhadra, K. and Keeton, C. Time delay and magnification centroid due to gravitational lensing by black holes and naked singularities. *Physical Review D*, 77(12):124014, 2008.

Virbhadra, K. S. and Ellis, G. F. Schwarzschild black hole lensing. *Physical Review D*, 62(8):084003, 2000.

Wands, D. Extended gravity theories and the einstein–hilbert action. *Classical and Quantum Gravity*, 11(1):269, 1994.

Zwicky, F. On the masses of nebulae and of clusters of nebulae. *The Astrophysical Journal*, 86:217, 1937.